

Redshift-Distance Survey of Early-Type Galaxies: Circular Aperture Photometry¹

M. V. Alonso^{1,2}, M. Bernardi³, L. N. da Costa^{4,5}, G. Wegner,⁶

C. N. A. Willmer^{5,7}, P. S. Pellegrini^{5,8} and M. A. G. Maia^{5,8}

¹Observatorio Astronómico de Córdoba, Laprida 854, Córdoba, 5000, Argentina and CONICET, Argentina

²CNRS UMR 5572, Observatoire Midi-Pyrénées, 14 Avenue E. Belin, 31400 Toulouse, France

³Department of Physics, Carnegie Mellon University, 5000 Forbes Ave., Pittsburgh, PA 15213, USA

⁴European Southern Observatory, Karl-Schwarzschild Strasse 2, D-85748 Garching, Germany

⁵Observatório Nacional, Rua General José Cristino 77, Rio de Janeiro, R. J., 20921, Brazil

⁶Department of Physics & Astronomy, Dartmouth College, Hanover, NH 03755-3528, USA

⁷UCO/Lick Observatory, University of California, 1156 High Street, Santa Cruz, CA 95064, USA

vicky@ast.obs-mip.fr (MVA)

Received November 17, 2018

Received _____; accepted _____

⁸Observatorio do Valongo, UFRJ, Ladeira do Pedro Antonio 43, Rio de Janeiro, R. J., 20080-090, Brazil

ABSTRACT

We present R-band CCD photometry for 1332 early-type galaxies, observed as part of the ENEAR survey of peculiar motions using early-type galaxies in the nearby Universe. Circular apertures are used to trace the surface brightness profiles, which are then fit by a two-component bulge-disk model. From the fits we obtain the structural parameters required to estimate galaxy distances using the $D_n - \sigma$ and Fundamental Plane relations. We find that about 12 % of the galaxies are well represented by a pure $r^{1/4}$ law while 87% are best fit by a two component model. There are 356 repeated observations of 257 galaxies obtained during different runs that are used to derive statistical corrections and bring the data to a common system. We also use these repeated observations to estimate our internal errors. The accuracy of our measurements are tested by the comparison of 354 galaxies in common with other authors. Typical errors in our measurements are 0.011 dex for $\log D_n$, 0.064 dex for $\log r_e$, 0.086 mag arcsec⁻² for $\langle \mu_e \rangle$ and 0.09 for m_{RC} , comparable to those estimated by other authors. The photometric data reported here represent one of the largest high-quality and uniform all-sky samples currently available for early-type galaxies in the nearby universe, especially suitable for peculiar motion studies.

Subject headings: cosmology: observations – galaxies: large-scale structure – galaxies: clustering – galaxies: photometry

¹Based on observations at Cerro Tololo Interamerican Observatory (CTIO), operated by the National Optical Astronomical Observatories, under AURA; European Southern Observatory (ESO); Fred Lawrence Whipple Observatory (FLWO); and the MDM Observatory on Kitt Peak.

1. Introduction

With the aim of mapping the distribution of total matter in the nearby Universe, we have completed a redshift-distance survey of early-type galaxies drawn from an all-sky magnitude-limited sample (hereafter ENEAR, da Costa et al. 2000a), which is being used to map the peculiar velocity field of galaxies in a volume of about 7000 km s^{-1} . The current survey extends the earlier effort of Lynden-Bell et al. (1988, hereafter 7S) by using a sample that is about three times larger, reaches more than one magnitude fainter, and also includes lenticular galaxies. In this paper we describe the measurements and present the results of the CCD photometry for the 1332 elliptical and lenticular galaxies that were measured in circular apertures for the ENEAR survey.

The peculiar velocity field of galaxies is a means of probing the total distribution of matter in the Universe within the gravitational instability framework. While other methods are known, in order to map the peculiar velocity field using galaxies, it is necessary to estimate distances that are independent of redshift; these distance determinations use scaling relations between spectroscopically measurable distance independent properties and photometrically defined distance dependent quantities such as radius or brightness. In addition, it is possible to compare independent determinations of the velocity field using different galaxy samples and distance determination techniques, which give strong support to the results. For example, the well known Tully-Fisher relation (hereafter TF, Tully & Fisher 1977, Mathewson et al. 1992, 1996, da Costa et al. 1996, Haynes et al. 1999a,b, Willick et al. 1997) has been extensively used to map the velocity field using spiral galaxies. Thus, employing early-type galaxies is a complementary analysis since a different observational technique is used and early-type and spiral galaxies probe different regions of space.

For early-type galaxies there are two scaling relations: (1) the Fundamental Plane (FP, Djorgovski & Davis 1987), a three dimensional space defined by surface brightness

($\langle \mu_e \rangle$), effective radius (r_e), and central velocity dispersion (σ) and (2) the $D_n - \sigma$ relation (Dressler et al. 1987, 7S) which correlates the characteristic size (D_n) with σ . The $D_n - \sigma$ relation which can be shown to be a projection of the FP (Jørgensen et al. 1993) is accurate over a range of $\langle \mu_e \rangle$ and it is easier to apply in practice. We have used the $D_n - \sigma$ relation to estimate distances and derive the peculiar velocity field for the ENEAR survey because D_n is simple to measure (it is obtained from an accurate interpolation, relying neither on fits to the galaxy light profiles nor on extrapolations) and it is as accurate as using r_e and $\langle \mu_e \rangle$ in the FP. Although, since the $D_n - \sigma$ relation is an approximation to the FP, it could introduce extra scatter in the measurements compared to using the FP. The resulting $D_n - \sigma$ relation can then be easily constructed using galaxies in clusters. The ENEAR template $D_n - \sigma$ relation, obtained from the subsample of galaxies in clusters, has been discussed in Bernardi et al. (2002a, 2002b), where the scatter in the present sample implies a distance error of about 19% per galaxy.

The photometric data reported here uses the CCD imaging of the ENEAR survey galaxies measured in circular apertures. Galaxy parameters for both $D_n - \sigma$ and the FP are determined using the Saglia et al. (1997) two-component disk-bulge model, which accounts for the smearing of light due to seeing and employs a sequence of $r^{1/4}$ and exponential profiles with appropriate scale lengths and disk-to-bulge ratios. The excellent fits achieved here using the two component model profile justify its use in determining the FP parameters.

As part of the papers of the series, the central velocity dispersion and line strengths of the galaxies obtained from the spectroscopic data of the survey are presented in Wegner et al. (2003). A number of results using the ENEAR data (photometric and spectroscopic data) have already appeared. These include statistical analyses of the ENEAR sample using the velocity correlation function (Borgani et al. 2000) and the dipole measurements

(da Costa et al. 2000b). These are in good agreement with the results obtained by the TF surveys, demonstrating that estimates of the cosmic flow as traced by early-type and spiral galaxies are statistically equivalent even though both galaxy types obey distinct distance relations and sample different density regimes, but probe the same induced peculiar velocity field. Nusser et al. (2001), examined the peculiar velocity field using the ENEAR galaxies and the PSCz gravity fields and showed that the likelihood analysis of the ENEAR and PSCz modes are in good agreement with the values obtained from the TF surveys. Further analyses include the measurement of the large-scale power spectrum obtained from the ENEAR peculiar velocity field (Zaroubi et al. 2001). In general, all these results suggest low-amplitude bulk flows and that most of the motion of the Local Group is due to mass fluctuations within the volume of 6000 km s^{-1} .

This paper is organized as follows: in Section 2, we describe the observational sample; in Section 3, we outline the procedure used to analyze the galaxy photometry, and assess the quality of our data. The photometric catalogue is presented in Section 4, while a summary of our main results concludes in Section 5.

2. The Data

2.1. The Sample

A detailed description of the ENEAR survey can be found in da Costa et al. (2000a) who describe the sample selection, properties and completeness, so we only present a brief overview here. The ENEAR sample was drawn from an all-sky source catalogue of galaxies of all types by selecting objects brighter than $m_{B(0)} = 14.5 \text{ mag}$ and with morphological types $T \leq -2$ (following the morphological classifications of Lauberts and Valentijn 1989) and with radial velocities $V_r \leq 7000 \text{ km s}^{-1}$; this sample will be referred to as ENEARm.

The distances were estimated with a template $D_n - \sigma$ relation (Bernardi et al. 2002a, 2002b) using the subsample of galaxies in 28 groups and clusters for which we use the name ENEARc. The galaxies were assigned to 23 of them by applying an objective group-finding algorithm to the source catalogue (which contains galaxies of all morphological types). We also added five additional well-studied clusters. This ENEARc subsample also contains 134 objects that are either fainter than $m_{B(0)} = 14.5$ or with $V_r > 7000 \text{ km s}^{-1}$. This means that while there is a considerable overlap between ENEARm and ENEARc neither sample contains the other in its entirety as a subset. In addition, while for the ENEARc sample (Bernardi et al. 2002a, 2002b), we combined our measurements with those of the literature, this paper reports only our new measurements.

The photometric data presented here consist of 1332 galaxies: 1104 objects belong to ENEARm, of which 201 are galaxies in clusters contained in the ENEARc sample. There are an additional 134 galaxies (with $m_{B(0)} > 14.5$ or with $V_r > 7000 \text{ km s}^{-1}$) belonging to ENEARc, as explained above and finally 94 galaxies that are contained in neither sample. Most of the latter are serendipitous early-type galaxies which lie in the same CCD frame as an observed programme galaxy, and generally have $V_r > 7000 \text{ km s}^{-1}$.

2.2. Observations

The R_C -band (Kron-Cousins) photometry reported in this paper was obtained over 100 photometric or partially photometric nights out of a total of 177, using several telescopes over various observing runs in the period 1987 – 1999. The following telescopes were employed: the Danish (hereafter DK) 1.54m and Dutch 0.9m telescopes at the European Southern Observatory (ESO); the 0.9m telescope at Cerro Tololo Interamerican Observatory (CTIO); the 0.61m and 1.3m telescopes at Fred Lawrence Whipple Observatory (FLWO) and the 1.3m telescope at MDM (formerly the Michigan–Dartmouth–MIT) Observatory.

The basic information for each run is summarized in Table 1 where we list: in column (1) the identification code of the run; in column (2) the observing date; in column (3) the number of the total/photometric nights and in column (4) the corresponding reference number of the instrumental setup, which is described in Table 2.

A total of 12 different setups were used, corresponding to different telescope/detector combinations and are described in Table 2 which gives: in column (1) the setup reference number; in column (2) the observatory and telescope identification; in columns (3) and (4) the total number of images observed in the R_C band (N_m) in that setup and the number of repeated images (N_r), which are used later as calibrators to homogenize our observations; and in columns (5) to (9) some characteristics of the detectors: identification, size, pixel scale, gain and read-out noise. It is important to mention that setups 3, 4 and 5 correspond to the DK 1.5m telescope with DFOSC (Danish Faint Object Spectrograph and Camera) and the CCDs identifications are reported in column (5).

Exposure times varied from 120 to 600 seconds depending on the telescope and the brightness of the galaxy. A total of 2339 images obtained under photometric conditions were analyzed. Of these, 2121 were taken with the R_C filter and 218 with B. The latter sample, comprising 178 galaxies, will be discussed in a separate paper (Alonso et al. 2003a). The final sample consisting of 1332 galaxies has been constructed after discarding 129 galaxies for a variety of reasons (e.g. superimposed objects; crowded fields) and about 50 galaxies observed too close to the edge of the CCD or with low signal-to-noise.

Finally, it is important to point out that we have a total of 257 objects with multiple observations using either the same or different setups. Given the long duration of the program and the large number of setups involved, these repeated observations are of paramount importance to ensure the overall uniformity of our data and were used to make our measurements of photometric parameters internally consistent and to estimate their

errors.

2.3. Data reduction and calibration

All images were trimmed, bias subtracted and flat-fielded using standard IRAF¹⁰ routines. The bias, dome and sky flats, obtained over one or more nights of a given run, were median combined and both sky flats and dome flats were used to investigate the quality of the flat-fielding. The uncertainty in the residual large-scale response of the CCD measured using the sky-flats was found to be less than 1%. No corrections for dark current were required as it was determined to be negligible for all detectors.

The photometric calibration relied on observations of Landolt (1983, 1992) standard stars in the Kron-Cousins R_C band and, depending on the run, in a second passband, generally V, but sometimes in B and I_C , to obtain color corrected solutions. In general, standards were observed at $\sim 1 - 2$ hour intervals, covering a wide range of colors and airmass throughout the night. Typically, about 30 stars were observed during each night. We followed the reduction procedure of Haynes et al. (1999b): instrumental magnitudes for the stars were obtained using a circular aperture large enough to measure the total flux without significantly increasing the error due to sky-noise. A suitable aperture was chosen for each run depending on the observed stellar fields, where we tried to minimize the rms obtained for the photometric solution in that run. Typical values of the aperture radii were ~ 6 arcsec. For the median seeing of 1.39 arcsec (see Figure 1) this is about 9 times larger than the point-spread function (hereafter PSF FWHM). The sky level was determined as the median value of counts measured within an annulus of about 16 arcsec radius centered

¹⁰IRAF (Image Reduction and Analysis Facility) is distributed by the National Optical Astronomy Observatories.

on the standard star, being far enough that the contribution from light in the stellar wings should be negligible.

The photometric solution was obtained for each night of a given run and mean values of the zero point and color term were taken for that run. Once they were fixed, the extinction coefficients were determined nightly for each run. Nights were considered photometric if the dispersion between the standard magnitudes and those obtained from the fits was $\lesssim 0.05$ mag. Using this criterion 94 out of the 177 nights allocated to the project were considered photometric. Six partially photometric nights were added after discarding the portions observed under unfavorable conditions. Since no colors are available for most of our galaxies, we have assumed mean colors of early-type galaxies as being $\langle B-R_C \rangle = 1.48$, $\langle V-R_C \rangle = 0.56$, and $\langle R_C-I_C \rangle = 0.70$ mag (Frei & Gunn 1994; Fukugita, Shimasaku & Ichikawa 1995). From the color terms for our nightly photometric solutions, which are typically 0.01, the uncertainty introduced by this assumption is of about 0.05 mag.

The distribution of the observed PSF FWHM, as measured from stars observed under photometric conditions off the same images as the program galaxies is shown in Figure 1. The median value of the distribution is ~ 1.39 arcsec but shows a tail extending to large values. Therefore, since the seeing FWHM is not always negligible compared to the sizes of the galaxies in the sample (see Section 3.2), all measurements of the photometric parameters were made on light profiles corrected for seeing.

3. Surface Brightness Profiles

The measurement of photometric and structural parameters of the galaxies employed the GALPHOT package originally developed for spiral galaxies (Haynes et al. 1999b and references therein). Background estimates were obtained from “sky boxes” placed in regions

around the galaxy that are free of bright stars, but far enough not to be contaminated by light coming from the outer parts of the galaxy or other resolved objects in the frame. For each “sky box” the mean intensity was computed after automatically masking out faint stars and galaxies within the box. The final sky value was computed as the mean of all values measured in the “sky boxes”, since the images were sufficiently flat. This average sky value was then subtracted from the image. The typical scatter of the mean sky intensity measured in each “sky box” was $\lesssim 0.5\%$.

Finally, prior to conducting the surface photometry, a rectangular region about twice the size of the galaxy image was marked and cosmic rays and stars outside this box were automatically masked. Standard IRAF routines were utilized to identify the different objects in the images above a given threshold and the classification of them was based on its roundness and sharpness. Stars which are within the rectangular region were not marked automatically to avoid eliminating important parts of the galaxy. Any remaining undesirable features both inside and outside the box were masked interactively. Masked stars and cosmic rays were not considered in calculations of the flux within different apertures.

We measured the surface brightness profiles of all galaxies using both circular and elliptical apertures. In both cases, the photometric center of the galaxy relied on the ellipse fitting method of Jedrzejewski (1987), from which one quantifies the shape and orientation of the galaxies, and the deviations of the isophotes from perfect ellipses. In this paper we only consider the profiles derived from circular apertures, and defer the discussion of the photometry using elliptical profiles to another paper (Alonso et al. 2003b).

3.1. Circular Averaged Aperture Profiles

The circularly averaged light profiles were measured using 1 pixel steps starting from an innermost radius of 1 pixel (ranging from 0.38 to 0.65 arcsec depending on the scale) to an outer radius r_{max} , where the light profile counts drop below the $1-\sigma$ level of the sky background. The center for the aperture photometry was assumed to be identical to the smallest ellipse derived from the two-dimensional isophotal fit (Alonso et al. 2003b). The instrumental values obtained for the surface brightness and magnitudes were calibrated using the photometric solution described in Section 2.3. The surface brightness profiles were also corrected by galactic extinction, the K -correction (Davis et al. 1985) and the $(1+z)^4$ cosmological effect. The galactic extinction in the R_C -band was estimated as $A_R = 0.58 A_B$ (Seaton 1979) where A_B was based on the maps of Burstein & Heiles (1984). The comparison of these extinction estimates with those of Schlegel, Finkbeiner & Davis (1998) gives a mean difference of -0.07 ± 0.05 , or a mean difference in A_R of about 0.04. For the observed galaxies, the galactic extinction correction is $A_R \lesssim 0.13$ mag.

The primary goal of our imaging survey has been to determine photometric quantities that can be used in the empirical distance relations, such as the $D_n - \sigma$ (Dressler et al 1987), to map the peculiar velocity field. The characteristic angular diameter D_n , as originally defined by the 7S, is the circular diameter within which the corrected average surface brightness of the galaxy is equal to $20.75 \text{ mag arcsec}^{-2}$ in the B band. The choice of isophotal level where D_n is defined is influenced by the presence of the disk. Using a faint isophotal level, especially in lenticular galaxies, may include a contribution from the disk component which can have different dynamical properties. At brighter isophotal levels the values are sensitive to seeing, especially for the more distant galaxies. If we follow Dressler (1987) who measures D_n at $19.75 \text{ mag arcsec}^{-2}$ in the B band for lenticular galaxies, we find very small values which are strongly affected by seeing. Moreover, in some studies (e.g.,

Jørgensen, Franx & Kjaergaard 1995, hereafter JFK and Lucey et al. 1991) the diameters have been measured at the same level independently of morphological type. Consequently in order to measure D_n , we adopt the isophotal level of $\mu_{RC} = 19.25 \text{ mag arcsec}^{-2}$ in the R_C -band regardless of the morphological type. This corresponds to the 7S B band definition assuming a mean color of $\langle \mu_B - \mu_{RC} \rangle = 1.5 \text{ mag arcsec}^{-2}$, which we obtained from galaxies in our sample observed in both bands.

The effective radius, r_e is the radius of the isophote that encloses half the luminosity of the galaxy bulge and $\langle \mu_e \rangle$ is the mean surface brightness within r_e . As we explain below, all these parameters are corrected for seeing effects (Saglia et al. 1993). The circularly averaged growth curves for most elliptical galaxies do not differ significantly from those derived from elliptical isophotes (Saglia et al. 1993). Both growth curves are equivalent when the surface brightness profile of a galaxy is described by a pure $r^{1/4}$ law and the ellipticity is constant. Even though most of the surface brightness profiles of early-type galaxies are a combination of bulge and disk components, the difference introduced by using circular apertures is small. In the cases of galaxies showing flattened bulges or an evident disk component, especially if they are seen edge-on, the values of the structural parameters are unreliable. These problems arise for objects with ellipticities > 0.6 (see Alonso et al. 2003b) which represent only a small fraction of the total ($\lesssim 4\%$).

3.1.1. *Quality of the profiles*

The internal accuracy was estimated using galaxies with more than one observation. Our sample includes 257 objects which have multiple observations obtained using either the same or different setups. The number of repeated observations ranges from 2 to 7: 206 objects were observed twice; 33 objects, 3 times; 10 objects, 4 times; 5 objects, 5 times; only 1 object, 6 times and 2 objects, 7 times. These repeat observations can be of three

different types: galaxies observed more than once during the same night; galaxies observed on different nights but using the same observational setup; galaxies observed with different setups. By splitting the comparisons in this way it is possible to evaluate the stability of the photometric solution over a night, quantify the impact of seeing variations and estimate our internal errors. Comparisons of galaxies observed on different nights are also useful since they reflect the more general cases of combining observations under different atmospheric conditions without introducing issues related to color-terms, field-of-view and other instrument and telescope dependent quantities. Finally, the comparisons between galaxies observed with different setups allow an evaluation of the zero-point calibration providing an additional check on the accuracy of our photometric solutions.

When making the comparison, we used the convention of performing the differences between "older minus newer" measurements. For instance, we compared a measurement taken at ESO-601 with all the other ESO runs. Then we compared ESO-603 measurements with later runs (e.g. ESO-604, ESO-605, ESO-606, etc. but not with ESO-601). The profiles were compared point by point and the mean weighted differences were computed using a range of radii (r_{min} and r_{max} , see above). This radial interval was chosen to avoid regions where the smearing of light due to seeing is significant, while the outer radius was chosen to minimize the contamination from other objects in the field. In general galaxies that present differences at large radii are either located in crowded stellar fields or have relatively bright stars superposed, so that an accurate mean sky level is difficult to measure. Other possible causes of large differences are residual contamination from nearby galaxies; and extended galaxies reaching the edge of the detector. At inner radii the center positions of the isophotes are very uncertain when there is light contamination by background stars, absorption features or when there is more than one surface brightness peak (probably dumb-bell systems). In the final comparisons we excluded objects that were flagged as contaminated or with uncertain sky subtraction. The complete set of plots with the

differences in the surface brightness profiles and a detailed description of the comparisons were presented by Bernardi (1999).

These results are summarized in Table 3 which gives: in column (1) the comparison set considered; in column (2) the number of different profiles being compared; in columns (3) the mean difference in surface brightness and error; and in column (4) the scatter. These values are consistent with those obtained from a similar comparison of profiles determined by the ellipse fitting procedure. The observed scatter in the comparisons are consistent with the accuracy of the photometric solutions ($\delta m \sim 0.05$ mag), giving a zero point estimate of about 0.037. The color term contribution to the surface brightness is, in general, smaller than $0.06 \text{ mag arcsec}^{-2}$. So, the larger scatter found in the comparison among different setups may reflect the uncertainties in the photometric calibration introduced by the zero point and different instrumental color terms.

3.2. Fitting procedure

3.2.1. Seeing corrections and Photometric Parameters

As our sample includes both elliptical and lenticular galaxies, we examine how the parameters involved in the scaling relations should be determined in the case of a two-component system. Following Saglia et al. (1997), the surface brightness profiles within circular apertures were fit using a two-component model comprising a bulge ($r^{1/4}$) and an exponential disk, convolved with a PSF FWHM (Saglia et al. 1993) to correct for seeing effects. The programs to make this seeing corrected profile decomposition were kindly provided by R. Saglia. The Fourier transform of the PSF FWHM is assumed to be $\approx \exp[-(kb)^\gamma]$, where b is a scaling parameter and γ is a parameter that describes the shape of the PSF FWHM. In general, γ varies between 1.3 for profiles with extended faint parts;

and 2 for profiles with a sharp cut. In our convolutions we assume $\gamma = 1.6$. The seeing can be significant out to a radius few times larger than the PSF FWHM, and thus lead to substantial errors when the ratio $r_e/(\text{PSF FWHM})/2$ is ~ 1 . Since the median seeing of our observations was ~ 1.4 arcsec and the median effective radius of the galaxies in the ENEARm sample is ~ 22 arcsec (as we will see below), seeing corrections are significant for $\lesssim 25\%$ of the galaxies. However, for faint ENEARc galaxies in clusters the seeing correction is important for at least half the observed galaxies.

Saglia et al. (1993) show that the presence of a disk component shifts galaxies away from the Fundamental Plane for elliptical galaxies. These deviations also correlate with the galaxy’s ellipticity, and will be discussed by Alonso et al. (2003b). Thus, in the present sample we use a two-component fit to the surface brightness profile, in contrast to some previous works (e.g., Burstein et al. 1987; JFK; Scodreggio et al. 1998) which used only a one-component fit to determine the photometric parameters used in the distance indicator. Saglia et al. (1997) also found that ignoring the disk component could bias the results leading to errors in r_e of $\sim 20\%$. However, by combining some of the galaxy parameters, the disk’s contribution can be sufficiently small so that its effect is canceled. Smith et al. (1997) employed this procedure by combining the effective radius with the mean surface brightness (using $\log r_e - 0.35 < \mu_e >$) which is little affected by the presence of a disk, since errors in r_e and $< \mu_e >$ are correlated. Our photometric data show no dependence of this quantity on the D/B ratio. Thus, using only the bulge component of lenticulars should not produce a tighter scaling relation for these galaxies, which is supported by the lack of any correlation in the $D_n - \sigma$ relation as a function of the D/B ratio (Bernardi et al. 2002a).

Each galaxy profile in our sample is fit three times using: (i) a pure $r^{1/4}$ law ($D/B = 0$); (ii) an exponential disk profile ($B/D = 0$); (iii) the sum of a bulge and a disk component. In all cases these profiles are convolved with the PSF FWHM as described above. The χ^2

is measured in the standard way, using the bulge effective radius (r_e); the disk exponential scale length (α); the disk-to-bulge ratio (D/B), and the seeing FWHM as fit parameters. The weights are the statistical errors in the values of the surface brightness at each radius. For each fit one can either assume a fixed mean sky value using “sky boxes” or allow it to be a fit parameter. Therefore, the method produces six sets of parameters. The χ^2 is computed for each of the six fits, and the one with the smallest reduced χ^2 is chosen as the best fit. Visual examination shows that in most cases the fit with the smallest χ^2 is reliable. However, in less than 1% of the cases we find that the best fit measured using χ^2 lead to artificially large disks. In these cases we use the results obtained from fits with slightly larger χ^2 but which are more consistent with the data profiles.

The FWHM as determined from the fits agree reasonably well with that measured from stellar profiles on the same galaxy frames. In Figure 2 we plot the comparison between the PSF FWHM measured both ways. The distribution peaks around zero but is skewed towards negative values indicating that, in general, the fitting procedure overestimates the seeing. The cases presenting large differences are due to poor fits, generally of galaxies observed in early runs using smaller CCDs or observations taken under poor conditions.

The seeing corrections make the overall galaxy light profile brighter and steeper in the innermost regions yielding structural parameters with larger D_n , brighter $\langle \mu_e \rangle$ and smaller r_e when compared to the uncorrected measures. The correction for D_n is only important for galaxies with $D_n \sim 10$ arcsec, which in the case of ENEARm affects only very few galaxies (see Figure 7). For values of $D_n > 10$ arcsec, D_n only increases by at most about 2%. However, the seeing corrections do become important for the ENEARc sample of galaxies in clusters, where the corrections can be as large as 20%.

3.2.2. The fit quality parameter Q

We assign a quality parameter Q to the profile fits adopting the method of Saglia et al. (1997) who use the following criteria: (i) the extent of the profile (r_{max}) relative to r_e ; (ii) the influence of seeing (the PSF FWHM compared to r_e); (iii) the value of the integrated galaxy S/N; (iv) the galaxy’s surface brightness relative to the sky; (v) the uncertainty in the sky determination; (vi) the fraction of the total light derived by extrapolating the profile beyond r_{max} used in the total magnitude m_{RC} ; (vii) the reduced χ^2 goodness-of-fit. The quality parameter ranges from excellent ($Q = 1$) to poor ($Q = 3$).

Monte-Carlo modeling of the EFAR sample enabled Saglia et al. (1997) to relate Q to the errors in the photometric parameters. Fits with $Q = 1$ led to the following errors: 1) $m_{RC} \lesssim 0.05$ mag; 2) $\log r_e \lesssim 0.04$; 3) $\log D_n$ and FP defined as $\log r_e - 0.30 < \mu_e > \lesssim 0.005$. For $Q = 2$ the respective errors are $\lesssim 0.15$ mag; ~ 0.11 and $\lesssim 0.01$. For $Q = 3$, the errors are larger than these values. Below we calibrate the errors in the ENEAR data and we find that our errors are comparable with those of Saglia et al. (1997).

Fit results of different quality are compared with the observed light profiles in Figures 3, 4 and 5. For each galaxy these figures show two panels: in the upper one, the observed light profile (small dots) and the fitted bulge and disc profiles (two solid lines) as a function of $r^{1/4}$ and in the lower panel, the difference in surface brightness $\Delta\mu = \mu_{obs}(r) - \mu_{fit}(r)$ (small dots, scale -0.2 to 0.2 mag arcsec⁻²) and the integrated magnitudes $\Delta m = m_{obs}(< r) - m_{fit}(< r)$ (solid line, scale -0.1 to 0.1 mag) derived from the observed and the fit profiles. The two differences are plot together but, for instance, the lower panel of NGC0128 (in Figure 3) is showing the scale and label corresponding to Δm and the lower panel of IC0100, the scale and label of $\Delta\mu$. The usefulness of Q to qualify the profile fits is evident in those cases of poor fits ($Q = 3$), where the inspection of the galaxy images shows the presence of spiral arms and/or bars, generally indicative of misclassifications

in the original catalogues. Cases showing large deviations from the fits are indicated in Table 6.

We have adopted the definitions of Saglia et al. (1997) for all Q parameters except for χ^2 which required renormalization to the S/N of our data in order to employ the results of their simulations. While Q indicates the quality of the fit and the resulting photometric parameters, it was only used to assess the profile fits. The final errors were estimated using galaxies with multiple observations and the accuracy of these errors were assessed using comparisons with other authors (see Section 3.3.3).

3.2.3. Results of Q measures for the ENEAR galaxies

The analysis of the profile fits for galaxies in ENEARm shows that $\sim 12\%$ are well described by the pure $r^{1/4}$ law while 87% are best fit by the two-component model, 78% of these cases having $D/B < 1$. Less than 1% of the galaxies have $D/B > 20$, and these usually show signs of nearby companions, spiral arms, etc. (see Table 6). For $\sim 26\%$ of the observed galaxies our results suggest that the morphological classifications in the source catalogues (all of which used photographic material) must be revised, as in most of these cases the CCDs with their larger dynamic range show the presence of bars and or spiral arms. Both the ENEARm and ENEARc samples include some disk-dominated galaxies.

For the ENEARm sample, 60% of the fits have $Q = 1$, 22% $Q = 2$, and 18% $Q = 3$. Most $Q = 3$ fits have relatively bright outer isophotal levels and truncated profiles. This not only impacts the Q s of the sky correction but also requires large radial extrapolations when computing the total magnitudes. The remaining poor fits ($\lesssim 30\%$) are caused by additional features in the light profiles as already described. For the ENEARc sample we find a higher percentage, 18%, of pure $r^{1/4}$ profiles. About 47% of the galaxies have $Q = 1$

fits, 27% $Q = 2$, and 26% $Q = 3$.

Figure 6 summarizes the parameters characterizing the light profile fit quality and the galaxy sample for the ENEARm and ENEARc, showing no significant differences between either samples. We found that the quality parameter $Q \leq 2$ for more than 80% of ENEARm galaxies and more than 70% for ENEARc galaxies (panel a). Furthermore, galaxies belonging to ENEARc tend to have slightly smaller D/B (panel b), and as expected smaller r_{max}/r_e (panel c) and smaller S/N (panel h). Consequently, the ENEARc fit qualities are slightly worse than in the case of ENEARm, since, in general, galaxies with smaller apparent sizes are more affected by seeing (panel d) and require larger extrapolations (panels c and i). However, this is not so evident in Figure 6 because the majority of the ENEARc galaxies (201 out of 335) belongs to ENEARm. The ENEARm is more uniform with slightly better fits as shown in panel (e). The calculation of total magnitudes requires extrapolations smaller than 10% in 70% (60%) of the cases for ENEARm (ENEARc) galaxies. Analogous plots may be seen in Saglia et al. (1997) for the EFAR sample of rather more distant clusters to $cz \sim 18,000 \text{ km s}^{-1}$. The differences between ENEAR and EFAR are apparent by comparing panels (a) and (e) with their equivalents in Saglia et al. (1997). Our sample contains brighter galaxies and we have a larger percentage of objects with the best quality fits. Also the differences with panels (b), (d) and (g) underline the difficulties of selecting true ellipticals of small apparent sizes. The seeing tends to bias the results for more distant samples as there is a preference in selecting higher surface brightness objects, when compared to the nearby samples.

3.3. Structural Parameters

3.3.1. Homogenization

When constructing the homogeneous data set of structural parameters used in the derivation of scaling relations, any remaining systematic shifts in the parameters were minimized using multiple observations of the same galaxies. We use the measurements obtained from images taken at ESO with setups 4 and 5 (see Table 2) as our fiducial system. These setups were chosen because they have the largest number of repeated observations using the same telescope, similar detectors, present the largest field of view and have the best resolution.

To determine the “fiducial” system we corrected our photometric parameters using the mean difference $\Delta y_i = \epsilon_i^2 \sum_{j \neq i} \sum_{k \in i, j} \frac{y_{ik} - y_{jk}}{\Delta y_{ik}^2 + \Delta y_{jk}^2}$ between the measurements of run i with all the other runs $j \neq i$ for galaxies in run j in common with those in run i . This offset is computed weighting by the variance which we take as being the estimated errors $\epsilon_i = \left(\sum_{j \neq i} \sum_{k \in i, j} \frac{1}{\Delta y_{ik}^2 + \Delta y_{jk}^2} \right)^{-1/2}$ in each measurement. Here k runs over the galaxies in common to runs i and j , and y_{ik} corresponds to the measurement of either D_n or r_e or $\langle \mu_e \rangle$ for galaxy k in run i and ϵ_{ik} is the estimated error.

We determined the most significant offset by finding the run with the maximum value $\Delta y_i / \sigma_i$, where σ_i is the standard error in the mean of run i , and iterated towards a common zero-point by subtracting this offset from the measurements of run i . We finished the process when the most significant offset was $\Delta y_i / \sigma_i < 2$. After three iterations the systematic offsets required to create a homogeneous fiducial data set were determined. In general, we found good agreement between the photometric parameters measured from repeated observations, so that the corrections required to bring them into a common system were relatively small: $\Delta \log D_n \lesssim 0.010$, $\Delta \langle \mu_e \rangle \lesssim 0.08 \text{ mag arcsec}^{-2}$, $\Delta \log r_e \lesssim 0.03$ and

$\Delta m_{RC} \lesssim 0.03$. In this process we discarded galaxies which exhibited peculiarities in their profiles as indicated by the comments in Table 6 (explained below).

After defining this standard system, the structural parameters derived from observations obtained at MDM, FLWO and CTIO were also transformed into it. For runs with a significant number of galaxies in common with our reference system, the measured values were directly compared, while other runs were corrected using the calibrated measurements for the same telescope. The corrections required for all data sets were small zero-point shifts, typically: $\Delta \log D_n \lesssim 0.003$, $\Delta \langle \mu_e \rangle \lesssim 0.04 \text{ mag arcsec}^{-2}$, and $\Delta \log r_e \lesssim 0.010$. These corrections are comparable to those found when defining the reference system.

3.3.2. Results

The structural parameters derived for the ENEARm and ENEARc samples are presented in Figures 7 and 8, where we show: in panel (a) the distribution of $\log D_n$ (*arcsec*); in panel (b) the distribution of $\log r_e$ (also in *arcsec*); in panel (c) the surface brightness distribution; in panel (d) the distribution of the total R_C - magnitudes; in panel (e) the relation between B magnitudes (from the literature), and our R_C magnitudes; and finally in panel (f) the $(B-R_C)$ colors.

Comparing these figures clearly shows the differences between the ENEARm and ENEARc samples, even though there is considerable overlap between them. As seen in panel (d) the ENEARm sample has a reasonably well-defined limiting magnitude at $R_C = 13.0$ which agrees well with the magnitude-limit adopted in the photographic B-selected sample where errors in the magnitudes can be as large as 0.5 mag (Alonso et al. 1993). While there is a linear relation between the B and R_C magnitudes, the scatter is large especially at the faint end. This is also seen in panel (f) where the mean colors are near 1.9. These differences

with the adopted color values of 1.48 to calibrate the photometry are mainly due to the fact that B magnitudes are photographic and the R_C magnitudes are obtained by the component luminosities of the fit decomposition. Colors redder than 2 indicate unreliable photographic B magnitudes or unreliable fits with higher extrapolations, the main source of uncertainties in m_{R_C} . The angular size of galaxies in the ENEARm (panels a and b), as measured either by D_n or r_e , is large, with a median of ~ 23 arcsec and ~ 17 arcsec, respectively. As discussed above, this means that the structural parameters for the ENEARm sample are rather insensitive to seeing, in contrast to the cluster ENEARc sample shown in Figure 8 that has median D_n and r_e values respectively of about 18 and 15 arcsec, with an extended tail towards smaller values. As the ENEARc is not a strictly magnitude-limited sample, galaxies can cover a wide range of apparent sizes, and thus present a wider distribution of structural parameters, specially in r_e (panel b). Finally, the distributions of the mean effective surface brightnesses are similar, peaking near ~ 19.5 mag arcsec $^{-2}$ in R_C but with a wider distribution in the ENEARc sample.

3.3.3. *Internal and External Comparisons: Errors*

In Figure 9 we compare the structural parameters of our repeated observations after applying the zero-point corrections. Again, we performed the differences using the convention "older minus newer" measurements, as explained in Section 3.1.1. We show, from top to bottom, the differences between the calibrated measurements of $\log D_n$, $\log r_e$, $\langle \mu_e \rangle$, FP and the total magnitude (m_{R_C}) observed at different sites (see figure caption). In the Figures, the dispersion in $\log D_n$ is smaller than for $\log r_e$ and $\langle \mu_e \rangle$. D_n is obtained by a simple interpolation while r_e and $\langle \mu_e \rangle$ result from fits where extrapolations are important. In the case of small CCDs, the extrapolations are the main source of uncertainties. The largest scatter in the photometric parameters occurs with FLWO data

but no single telescope set has a much larger uncertainties than the others. Figure 10 shows the distribution of the differences of all the compared parameters. The correlation of the differences in $\log r_e$ and $\langle \mu_e \rangle$ is shown in panel (a). The solid line shows the relation $\log r_e = 0.27 \langle \mu_e \rangle$ in good agreement with JFK results. The histograms of the differences are shown in (Panel b) $\log D_n$, (Panel c) $\log r_e$, (Panel d) $\langle \mu_e \rangle$, (Panel e) FP and (Panel f) m_{RC} . The distribution of differences in FP is broader than the distribution of the differences in $\log D_n$.

Table 4 summarizes the results of these comparisons which gives: in column (1) the site; in columns (2) the number of repeated measurements N_{D_n} in that site or in common with our standard system; in column (3) the mean offset and error of $\log D_n$; and in column (4) its scatter. In the remaining columns the same information, including the number of repeated measurements N_{FP} , is given for $\log r_e$, $\langle \mu_e \rangle$, FP and m_{RC} . These results are comparable to those internal estimates by JFK.

We transformed all the photometric data into the fiducial system and combined the individual measurements weighting by the errors in the cases of multiple observations. For each value of D_n the error was computed taking into account the uncertainties associated with the quality of the fits, and the rms scatter σ_{D_n} measured from multiple observations of galaxies obtained using the same telescope. These errors include the contribution from the photometric calibration because they were scaled from the internal comparisons. Its effect was also estimated from Monte-Carlo simulations where a number of light profile shapes covering the range of magnitudes and D/B ratios observed in the ENEAR sample were generated. For each of these galaxy profiles, 100 simulations were created by shifting the photometric zero-point by an offset drawn from a Gaussian deviate with a dispersion equal to the estimated zero-point error of the calibration. For each of these simulated profiles the photometric parameters were calculated and their mean and scatter were computed. This

was done for a range of *rms* values up to 0.05 mag, the value we adopted for a photometric night. We found that the errors in D_n depend on the profile shape, and the zero-point errors lead to uncertainties which are comparable to those estimated for high quality profiles (see Bernardi 1999, for details). Therefore, we prefer to estimate the final errors for D_n taking into account the quality of the fit and the scatter of the internal comparisons.

The same procedure was applied to derive errors for the other parameters, but in these cases the main contribution is the uncertainty associated with the quality of the fits. The distribution of all error parameters of interest ($\log D_n$, $\log r_e$, $\langle \mu_e \rangle$, and m_{RC}), is shown in Figure 11 for galaxies in the ENEARm sample. The median errors are 0.011 dex for $\log D_n$, 0.064 dex for $\log r_e$, 0.086 mag arcsec⁻² for $\langle \mu_e \rangle$ and 0.09 mag for m_{RC} .

The accuracy of our measurements was tested by comparing our structural parameters with those of other authors. Altogether there are 354 galaxies in our sample in common with Dressler (1987); Lucey & Carter (1988); Faber et al. (1989); Dressler, Faber & Burstein (1991); JFK; Lucey et al. (1997); and Smith et al. (1997). The largest overlaps are with Faber et al. (1989), with whom we have 293 galaxies in common, and JFK with 232 galaxies. These comparisons are shown in Figure 12. Because the errors in r_e and $\langle \mu_e \rangle$ correlate strongly (Jørgensen et al. 1996) and they are sensitive to the fitting procedure adopted by different authors, we also present the comparison for the photometric components of the FP, that is $\log r_e - 0.30 \langle \mu_e \rangle$. Not all parameters are available in the literature, especially in the case of those derived from profile fits.

The results of these comparisons are presented in Table 5 listing the literature source; the number of galaxies used in the D_n comparison; the differences, error and scatter for D_n ; the number of galaxies used in the comparisons of r_e , $\langle \mu_e \rangle$ and FP and the differences, error and scatter, respectively. In the D_n comparison, all the values are defined in the B-band isophotal level and the results are consistent with this assumption. The larger offset

in the comparison of $\log D_n$ with 7S and Dressler (1987) values was also found by JFK. The differences observed with JFK for the FP parameters, specially an offset of about 0.4 in $\langle \mu_e \rangle$, reflect the color term introduced between their Gunn r data and our Kron-Cousins photometry. Taking into account that there is a mean difference in magnitudes of $r-R_C$ of about 0.354 mag (Jørgensen 1994) and in $\log r_e$ of -0.014 (Table 5), it is straightforward to find a difference in $\langle \mu_e \rangle$ of 0.424, in agreement with our results. A similar offset was also found by Smith et al. (1997) in their comparisons with JFK. With them we are in the same system and all the galaxies we have in common are in the central parts of clusters. The observed difference in the $\langle \mu_e \rangle$ comparison is due mainly to strong light contamination from nearby galaxies, giving a difficult sky subtraction and more uncertain fit results. Once again, D_n is obtained in the inner parts and the light contamination is not so important. The observed scatter in D_n in all cases is nearly the same, ~ 0.025 , consistent with our internal error estimates (~ 0.023), if we assume that our errors and those of the other authors are of the same amplitude. The scatter for the other parameters in the comparisons with JFK is consistent with their results for external comparisons and also with Saglia et al. (1997) results.

4. The ENEAR Photometric Catalogue

The final catalogue listing structural parameters for 1332 galaxies is presented in Table 6. The Table comprises 1104 galaxies in the ENEARm sample; 335 in ENEARc, of which 201 are also contained in ENEARm; and 94 galaxies with later morphological types, as explained in Section 2.1. The Table gives in column (1) the galaxy identifications from NGC, IC, ESO, MCG, UGC catalogs. For galaxies in clusters not in these catalogs, we use D from Dressler (1980), RH and RK (Hydra cluster and Klemola 27, respectively from Richter 1989), WA and WS (Abell 3574–Klemola 27 and S753, respectively from

Willmer et al. 1991), J from JFK, ZH from Zwicky & Humason (1964) and L from Lucey et al. (1991). The Table also lists in columns (2)-(3) the 2000 equatorial coordinates; in columns (4) the morphological type T (Lauberts & Valentijn 1989); (5) $B(0)$ magnitude and (6) radial velocity, all from the literature; in column (7) the number of our observations; in columns (8)-(9) the total R_C -band magnitude and its error; in columns (10)-(15) the same information for $\log D_n$ (D_n in arcmin/0.1); $\log r_e$ (r_e in arcsec) and $\langle \mu_e \rangle$ (in mag/arcsec²), respectively; in column (16) the D/B ratio; in column (17) the FWHM of the point-spread function (in arcsec) determined from the fit; in column (18) are notes describing features observed in the galaxy light profile which may affect the determination of the photometric parameters; and in column (19) the galaxies previously observed by other authors (indicated with an asterisk). The column containing the notes also identifies objects that may have to be excluded in analyses requiring reliable photometric parameters, such as the derivation of galaxy distances, one of our primary goals.

5. Summary

We have presented structural parameters derived from the surface photometry for 1332 early-type galaxies as part of the ENEAR project. These galaxies have been used in previous papers of this series to probe the peculiar velocity field in a volume within 7000 km s⁻¹. The present sample represents a wide-angle photometric survey of early-type galaxies brighter than $m_{B(0)} = 14.5$ mag, which extends the 7S sample both in morphological types and depth. It also complements the recently completed TF surveys of spiral galaxies (Mathewson et al. 1992, 1996, da Costa et al. 1996, Haynes et al. 1999 a,b) for studies of the peculiar velocity field in the nearby Universe.

The surface brightness profiles have been obtained from circular apertures, and have been fit by a seeing-convolved two-component bulge-disk model to derive structural

parameters such as D_n , r_e and $\langle \mu_e \rangle$. We evaluate the quality of the data comparing the profiles and structural parameters obtained from multiple observations of individual galaxies. These multiple observations were also used to bring the photometric parameters into a common, homogeneous fiducial system. The corrections were relatively small: $\Delta \log D_n \lesssim 0.003$, $\Delta \langle \mu_e \rangle \lesssim 0.04 \text{ mag arcsec}^{-2}$, and $\Delta \log r_e \lesssim 0.010$. The errors in the structural parameters estimated from the scatter of internal comparisons are: 0.011 dex in $\log D_n$, 0.064 dex in $\log r_e$, 0.086 mag arcsec^{-2} in $\langle \mu_e \rangle$ and 0.09 for m_{RC} . The comparison of our photometric data for galaxies in common with other authors shows good agreement and confirms that our internal error estimates are fairly robust.

From the profile fitting we found that about 12 % of the galaxies are well represented by a pure $r^{1/4}$ law while 87% are best fit by a two component model. In the original morphological classification of the galaxies there are about 26% of ellipticals. In general we find that 60% of ENEARm galaxy profiles are of high quality, while for galaxies in clusters (ENEARc) this number decreases to about 47%. The derived photometric parameters have been used, in conjunction with the spectroscopic data (Wegner et al. 2003), in previous papers of this series to derive reliable distances and map the peculiar velocity field in the nearby Universe.

Acknowledgements

We would like to thank the anonymous referee to help us to improve the text with constructive comments. MVA would like to thank Wolfram Freudling, Inger Jørgensen, David Latham, Alejandra Milone, Reynier Peletier, and Ivo Busko for their contributions during different phases of this project. MVA and MB thank Roberto Saglia for providing and assisting us with the program to obtain seeing corrected decompositions of the profiles. MVA would like to thank the hospitality of the Harvard–Smithsonian Center for Astrophysics, the ESO visitor program and ON where much of the work was carried out. We

wish to thank the support of the CNPq–NSF bilateral program (MVA, LNdC), a research fellowship from CNPq (PSSP) and CLAF (MVA, PSSP and MAGM) for financial support to the project. MB also thanks the Sternwarte München, the Technische Universität München, ESO Studentship program, and MPA Garching for their financial support during different phases of this research. GW acknowledges support from the following over the course of this project: Dartmouth College, the Alexander von Humboldt-Stiftung for a year’s stay at the Ruhr Universität in Bochum, and ESO for supporting trips to Garching. MVA also acknowledges financial support from the SECYT and CONICET (Argentina). CNAW acknowledges partial support from CNPq grants 301364/86-9, 453488/96-0, and NSF AST-9529028 and NSF AST-0071198

REFERENCES

- Alonso, M. V., da Costa, L. N., Pellegrini, P. S. & Kurtz, M. J. 1993, *AJ*, 106, 676
- Alonso, M. V. et al. 2003a, in preparation
- Alonso, M. V. et al. 2003b, in preparation
- Bernardi, M. 1999, PhD Thesis, Ludwig–Maximilians– Universität, München
- Bernardi, M., Alonso, M. V., da Costa, L. A., Willmer, C. N. A., Wegner, G., Pellegrini, P. S., Rit e, C., & Maia, M. A. G. 2002a, *AJ*, 123, 2159
- Bernardi, M., Alonso, M. V., da Costa, L. A., Willmer, C. N. A., Wegner, G., Pellegrini, P. S., Rit e, C., & Maia, M. A. G. 2002b, *AJ*, 123, 2990
- Borgani, S., Bernardi, M., da Costa, L. N., Wegner, G., Alonso, M. V., Willmer, C. N. A., Pellegrini, P. S. & Maia, M. A. G. 2000, *ApJL*, 537,1
- Burstein, D. & Heiles, C. 1984, *ApJS*, 54, 33
- Burstein, D., Davies, R. L., Dressler, A., Faber, S. M., Stone, R. P. S., Lynden-Bell, D., Terlevich, R. J. & Wegner, G. 1987, *ApJS*, 64, 601
- Davis, L., Cawson, M., Davies, R. L., & Illingworth, G. D. 1985, *AJ*, 90, 169
- da Costa, L. N., Freudling, W., Wegner, G., Giovanelli, R., Haynes, M. P. & Salzer, J. J. 1996, *ApJ*, 468, L5
- da Costa, L. N., Bernardi, M., Alonso, M. V., Wegner, G., Willmer, C. N. A., Pellegrini, P. S., Rit e, C. & Maia, M. A. G. 2000a, *AJ*, 120, 95
- da Costa, L. N., Bernardi, M., Alonso, M. V., Wegner, G., Willmer, C. N. A., Pellegrini, P. S., Maia, M. A. G., Zaroubi, S. 2000b, *ApJL*, 537, 81

- Djorgovski, S. & Davis, M. 1987, ApJ, 313, 59
- Dressler, A. 1980, ApJS, 42, 565
- Dressler, A., Lynden–Bell, D., Burstein, D., Davies, R. L., Faber, S. M., Terlevich, R. J. & Wegner, G. 1987, ApJ, 313, 42
- Dressler, A. 1987, ApJ, 317, 1
- Dressler, A., Faber, S. M. & Burstein, D. 1991, ApJ, 368, 54
- Faber, S. M., Wegner, G., Burstein, D., Davies, R. L., Dressler, A., Lynden-Bell, D. & Terlevich, R. J. 1989, ApJS, 69, 763
- Frei, Z. & Gunn, J. E. 1994, AJ, 108, 1476
- Fukugita, M., Shimasaku, K. & Ichikawa, T. 1995, PASP, 107, 945
- Haynes, M. P., Giovanelli, R., Chamaraux, P., da Costa, L. N., Freudling, W., Salzer, J. J., & Wegner, G. 1999a, AJ, 117, 2039
- Haynes, M. P., Giovanelli, R., Salzer, J. J., Wegner, G. Freudling, W., da Costa, L. N., Herter, T., & Vogt, N. P. 1999b, AJ, 117, 1668
- Jedrzejewski, R. I. 1987, MNRAS, 226, 747
- Jørgensen, I., Franx, M. & Kjaergaard, P. 1993, ApJ, 411, 34
- Jørgensen, I. 1994, PASP, 106, 967
- Jørgensen, I., Franx, M. & Kjaergaard, P. 1995, MNRAS, 273, 1097 (JFK)
- Jørgensen, I., Franx, M. & Kjaergaard, P. 1996, MNRAS, 280, 167
- Landolt, A. 1983, AJ, 88, 439

- Landolt, A. 1992, *AJ*, 104, 340
- Lauberts, A., & Valentijn, E. A. 1989, *The Surface Photometry Catalogue of the ESO–Uppsala Galaxies (Garching:ESO)*
- Lucey, J. R., Carter, D. 1988, *MNRAS*, 235, 1177
- Lucey, J. R., Bower, R. G. & Ellis, R. S. 1991, *MNRAS*, 249, 755
- Lucey, J. R., Guzman, R., Steel, J. & Carter, D. 1997, *MNRAS*, 291, 488
- Lynden–Bell, D., Faber, S.M., Burstein, D., Davies, R.L., Dressler, A., Terlevich, R.J., & Wegner, G. 1988, *ApJ*, 326, 19 (7S)
- Mathewson, D. S., Ford, V. L., & Buchhorn, M. 1992, *ApJS*, 81, 413
- Mathewson, D. S., & Ford, V. L. 1996, *ApJS*, 107, 97
- Nusser, A., da Costa, L. N., Branchini, E., Bernardi, M., Alonso, M. V., Wegner, G., Willmer, C. N. A. & Pellegrini, P.S. 2001, *MNRAS*, 320, L21
- Richter, O.-G. 1989, *A&AS*, 77, 237
- Saglia, R. P., Bertschinger, E., Baggley, G., Burstein, D., Colles, M., Davies, R. L., McMahan, Jr., R. K. & Wegner, G. 1993, *MNRAS*, 264, 961
- Saglia, R. P., Bertschinger, E., Baggley, G., Burstein, D., Colles, M., Davies, R. L., McMahan, Jr., R. K. & Wegner, G. 1997, *ApJS*, 109, 79
- Seaton, M. J. 1979, *MNRAS*, 187, 73
- Scodreggio, M., Giovanelli, R. & Haynes, M. P. 1998, *AJ*, 116, 2728
- Schlegel, D. J., Finkbeiner, D. P. & Davis, M. 1998, *ApJ*, 500, 525

Smith, R. J., Lucey, J. R., Hudson, M. J. & Steel, J. 1997, MNRAS, 291, 461

Tully, R. B. & Fisher, J. R. 1977, A. & A., 54, 661

Wegner, G. et al. 2003, in preparation

Willick, J. A., Strauss, M. A., Dekel, A., & Kolatt, T. 1997, ApJ, 486, 629

Willmer, C. N. A., Focardi, P., Chan, R., Pellegrini, P. S., da Costa, Nicolaci L. 1991, AJ,
101, 57

Zaroubi, S., Bernardi, M., da Costa, L. N., Hoffman, Y., Alonso, M. V., Wegner, G.,
Willmer, C. N. A., Pellegrini, P. S. 2001, MNRAS, 326, 375

Zwicky, F. & Humason, M. L. 1964, ApJ, 139, 269

Table 1: Observing Runs for Photometry

Run	Date	N_{tp}	Setup
(1)	(2)	(3)	(4)
CTIO-701	Nov 87	5/3	9
FLWO-201	Dec 88	15/0	7
FLWO-202	Apr 89	11/8	7
FLWO-203	Sep 89	9/6	7
ESO-601	Nov 89	4/4	1
CTIO-702	sep 90	2/0	9
FLWO-204	Nov 91	4/0	8
ESO-602	Sep 92	4/0	1
FLWO-205	Oct 92	6/2	8
MDM-551	Jan 93	4/0	10
FLWO-206	Mar 93	4/3	8
ESO-603	Jul 93	5/3+1	2
ESO-604	Nov 93	4/2+2	2
ESO-605	May 94	7/5	2
MDM-552	Mar 95	7/5+1	11
ESO-606	Aug 95	2/2	3
MDM-553	Nov 95	7/6+1	12
ESO-611	Dec 95	16/15	6
MDM-555	May 96	3/3	12
ESO-607	Oct 96	3/0	4
MDM-554	Nov 96	8/0	12
ESO-608	Feb 97	3/3	4
MDM-556	Feb 97	6/3	12
ESO-609	Apr 97	4/4	5
MDM-557	Jun 97	4/3	12
ESO-610	Nov 97	4/1	5
MDM-558	Nov 97	4/0	12
ESO-613	Mar 98	3/3	5
MDM-559	May 98	4/3	12
MDM-560	Nov 98	1/1	12
CTIO-703	Feb 99	7/6+1	10
CTIO-704	Sep 99	7/0	10

Notes: In column (3) is reported the number of the total/photometric nights for the corresponding run. This column also includes the number of partially photometric nights, preceded by a plus sign. Information about the setup indicated in column (4) are given in Table 2

Table 2. Observing Setups

Setup	Telescope	N_m	N_r	Detector	Field of View arcmin \times arcmin	Scale arcsec/pixel	Gain e^-/ADU	RON [e^-]
1	DK 1.54m	36	8	RCA 5264-7-3	4.0×2.5	0.47	20	15
2	DK 1.54m	414	61	Tek #28	6.5×6.5	0.38	3.5	8.0
3	DK 1.54m	153	44	CCD #17	8.5×8.5	0.51	2.0	3.7
4	DK 1.54m	96	17	LORAL/LESSER W11-4	13.3×13.3	0.39	1.31	7.2
5	DK 1.54m	304	54	LORAL/LESSER C1W7	13.3×13.3	0.39	1.31	7.2
6	Dutch 0.9m	50	21	Tek	3.8×3.8	0.44	3.56	8.0
		1053	205					
7	FLWO 0.61m	85	8	Tek	5.5×5.5	0.65	3.8	12
8	FLWO 1.3m	228	45	Tek	11.2×11.2	0.65	2.5	13
		313	53					
9	CTIO 0.9m	47	26	RCA # 5	4.2×2.6	0.49	6.5	–
10	CTIO 0.9m	247	42	Tek2K	13.5×13.5	0.396	3.2	4.0
		294	68					
11	MDM 1.3m	48	4	Wilbur LORAL binned 2×2	10.5×10.5	0.63	2.25	4.73
12	MDM 1.3m	413	26	Nellie STIS	15.0×15.0	0.44	2.94	4.38
		461	30					
Total		2121	356					

Notes: In columns (3) and (4) are listed the total number of images observed in the R_C band (N_m) in the different setups and the number of repeated images (N_r) for that setup, which are used as calibrators to homogenize our observations.

Table 3: Internal Comparisons of the Light Profiles

Comparison	N_c	$\Delta\mu$ mag/arcsec ²	σ_μ mag/arcsec ²
same night	172	0.004 ± 0.003	0.042
same setup	53	0.001 ± 0.007	0.052
different setups	114	0.002 ± 0.009	0.094

Table 4: Internal Comparisons of the Structural Parameters

Site	N_{D_n}	$\Delta \log D_n$ arcmin/0.1	$\sigma_{\log D_n}$	N_{FP}	$\Delta \log r_e$ arcsec	$\sigma_{\log r_e}$	$\Delta \langle \mu_e \rangle$ mag/arcsec ²	$\sigma_{\langle \mu_e \rangle}$	ΔFP	σ_{FP}	Δm_{RC} mag	$\sigma_{m_{RC}}$
ESO	118	-0.001±0.002	0.023	82	-0.013±0.010	0.089	-0.074±0.036	0.327	0.010±0.003	0.024	-0.001±0.014	0.129
MDM	88	-0.005±0.002	0.020	63	0.006±0.013	0.100	0.016±0.046	0.365	0.001±0.003	0.023	0.001±0.017	0.132
FLWO	43	-0.002±0.002	0.014	29	0.021±0.017	0.092	0.083±0.064	0.346	-0.004±0.003	0.018	-0.019±0.025	0.133
CTIO	64	-0.005±0.002	0.017	55	0.008±0.013	0.094	0.025±0.046	0.343	0.001±0.003	0.021	-0.012±0.017	0.126

Table 5: External Comparisons of the Structural Parameters.

Sources	N_{D_n}	$\Delta \log D_n$ arcmin/0.1	$\sigma_{\log D_n}$	N_{FP}	$\Delta \log r_e$ arcsec	$\sigma_{\log r_e}$	$\Delta \langle \mu_e \rangle$ mag/arcsec ²	$\sigma_{\langle \mu_e \rangle}$	ΔFP	σ_{FP}
LC	84	0.003 ± 0.003	0.027
7S	293	0.013 ± 0.002	0.034
D	54	0.016 ± 0.004	0.027
JFK	232	0.002 ± 0.002	0.023	210	-0.014 ± 0.008	0.116	-0.410 ± 0.030	0.431	0.109 ± 0.003	0.039
Lc	13	-0.004 ± 0.004	0.015
S	15	0.005 ± 0.009	0.034	13	-0.074 ± 0.026	0.095	-0.306 ± 0.103	0.372	0.018 ± 0.011	0.041

Notes: All differences are “our measurement” - “literature measurement”.

The references are LC: Lucey & Carter (1988); 7S: Faber et al. (1989); D: Dressler (1987) and Dressler, Faber & Burstein (1991); JFK: Jørgensen, Franx, & Kjærgaard (1995); Lc: Lucey et al. (1997); S: Smith et al. (1997)

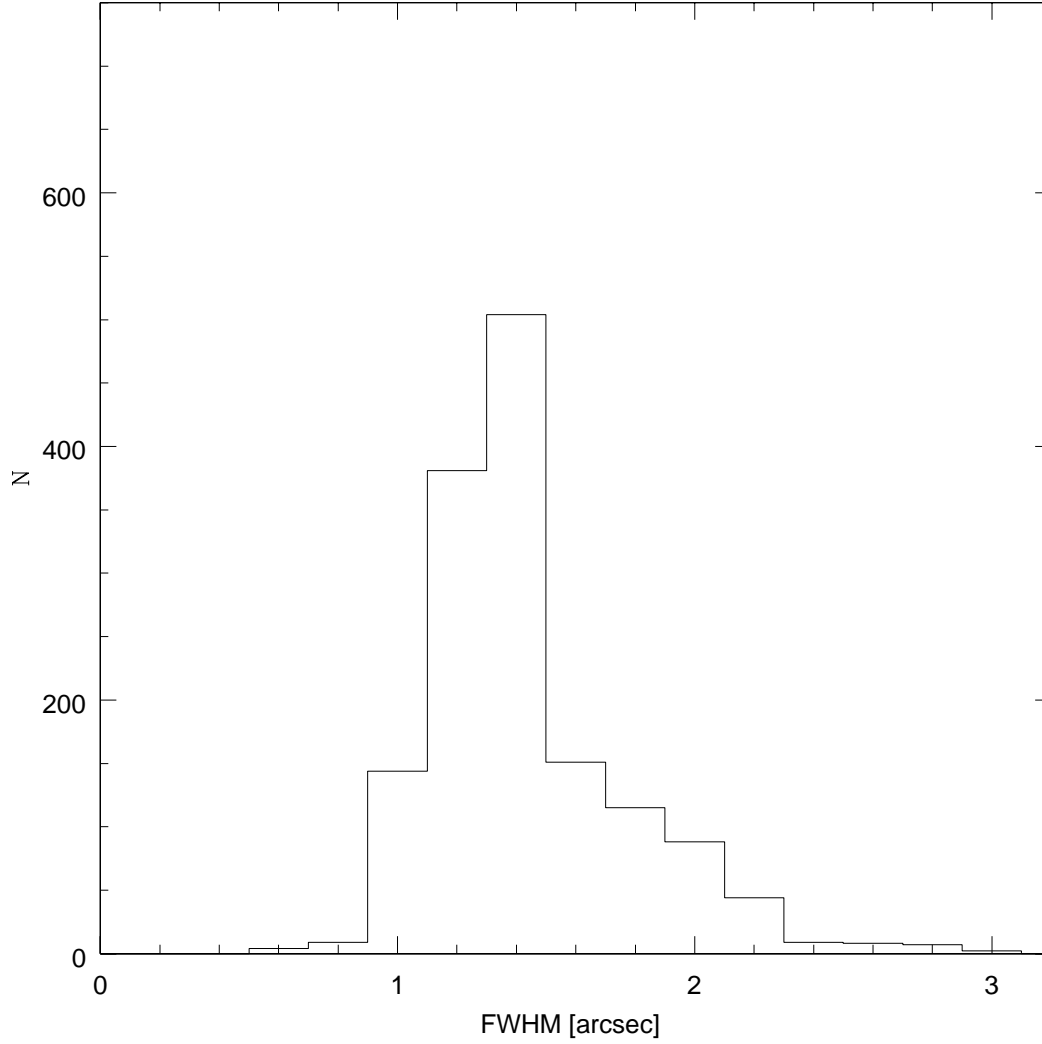


Fig. 1.— Distribution of the PSF FWHM values in arc seconds, as measured from stars observed in the same images as the programmed galaxies. The median seeing is ~ 1.39 arcsec. The distribution is skewed to high values, which are mostly caused by observations made under unfavorable conditions.

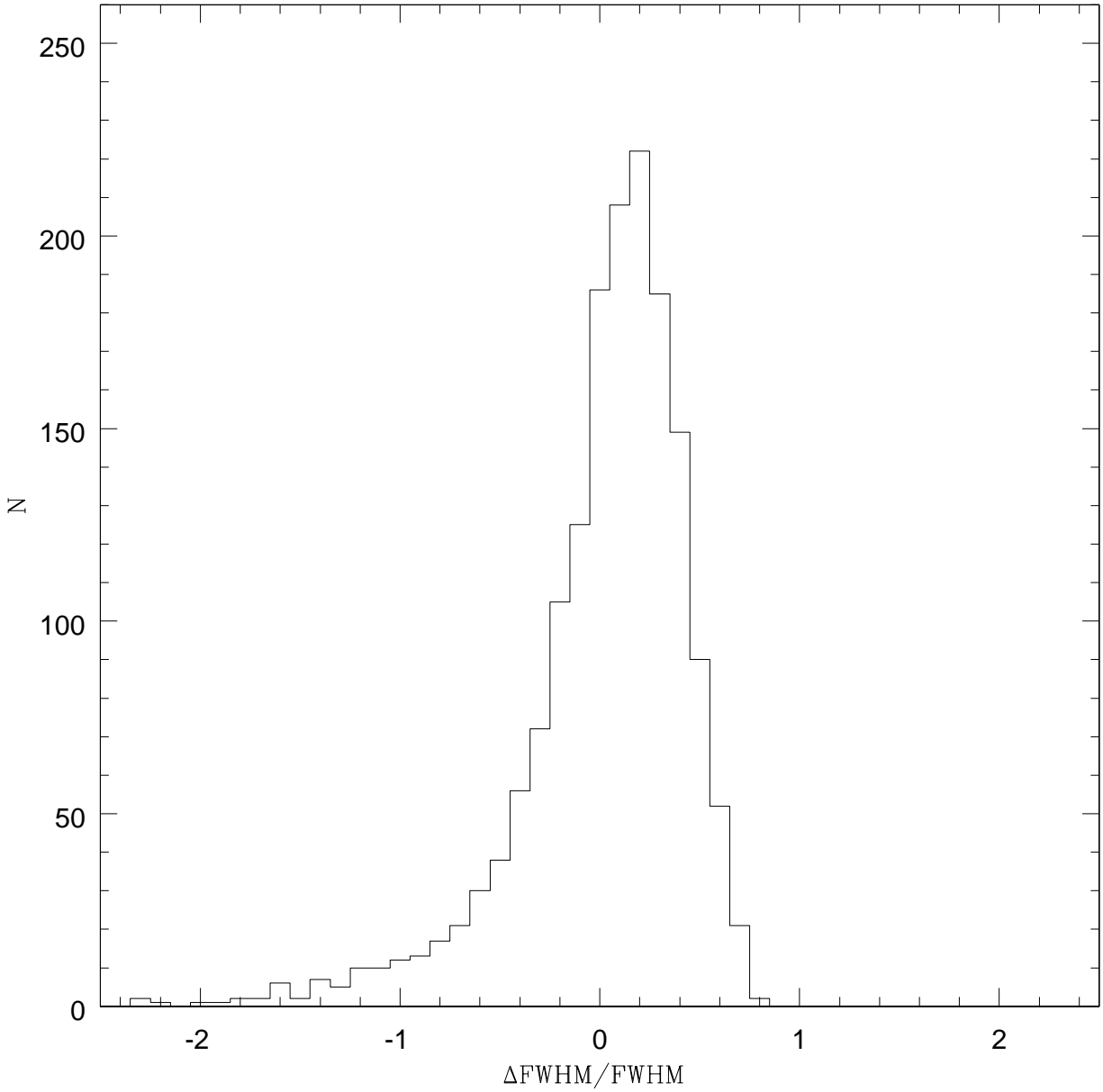


Fig. 2.— The distribution of the $\Delta \text{FWHM} / \text{FWHM}$ (measured), where $\Delta \text{FWHM} = \text{FWHM}(\text{measured}) - \text{FWHM}(\text{fit})$.

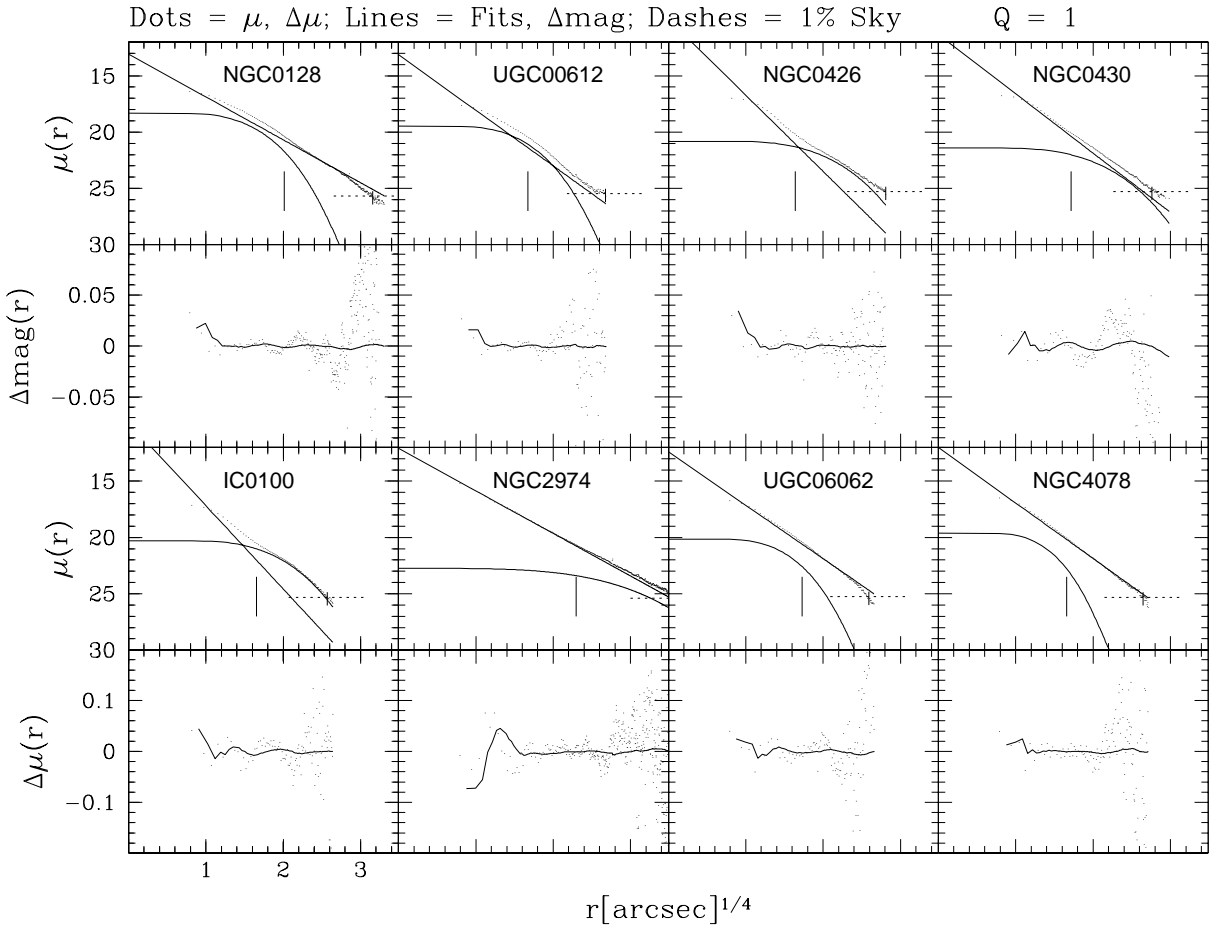


Fig. 3.— Examples of the light profile fitting of excellent quality ($Q = 1$). For each galaxy there are two plots showing: in the upper panel, the observed light profile (small dots) and the best-fit (solid lines) as a function of $r^{1/4}$. The larger vertical line marks the derived value of r_e , while the smaller shows the maximum extent of the profile, r_{max} . The horizontal dashed line is the intensity corresponding to 1% of the sky. The lower panel shows the differences $\Delta\mu = \mu_{obs}(r) - \mu_{fit}(r)$ (small dots) and $\Delta m = m_{obs}(< r) - m_{fit}(< r)$ (solid line).

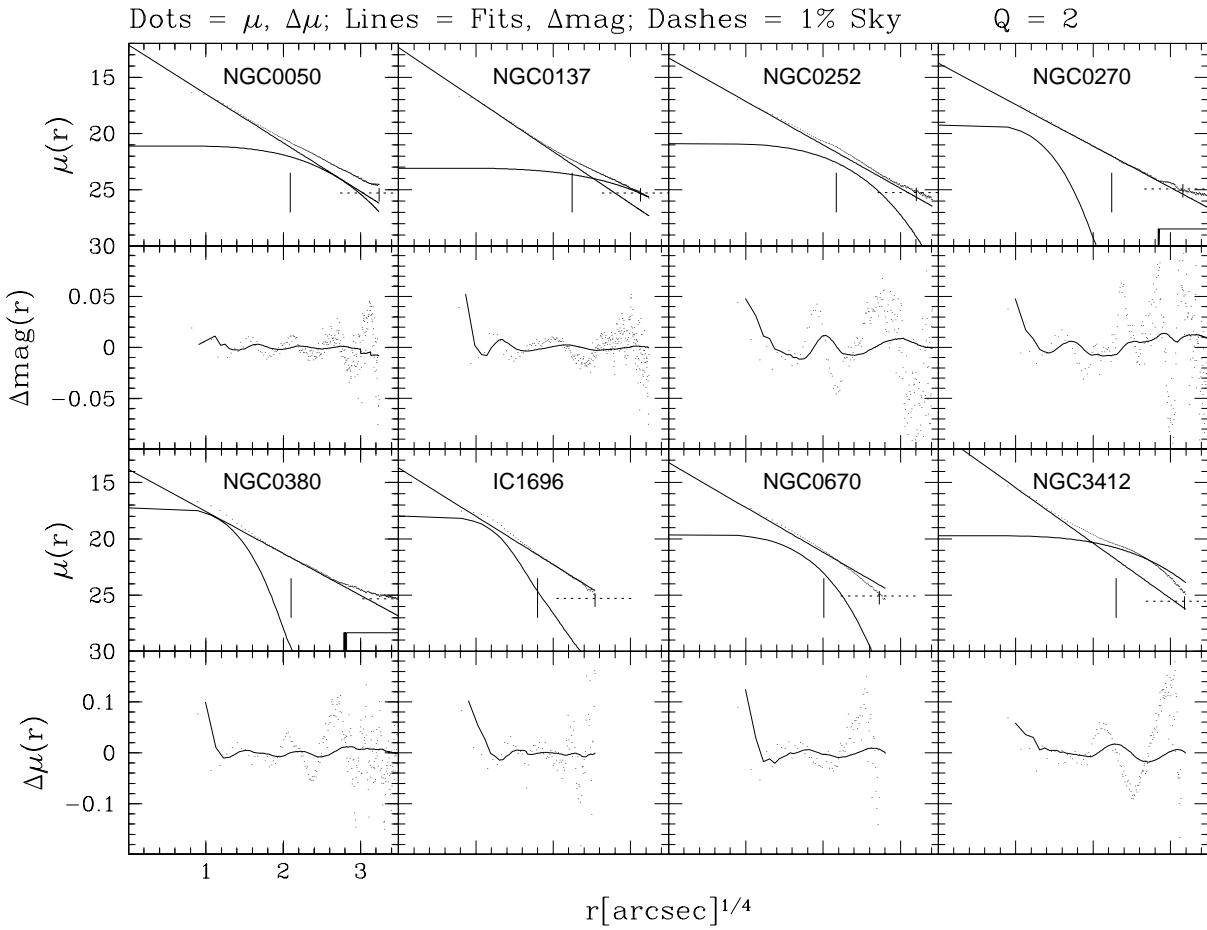


Fig. 4.— Examples of the light profile fitting of moderate quality ($Q = 2$). The two panels for each galaxy show the observed light profile, the best fit and differences in surface brightness and magnitudes as in Figure 3.

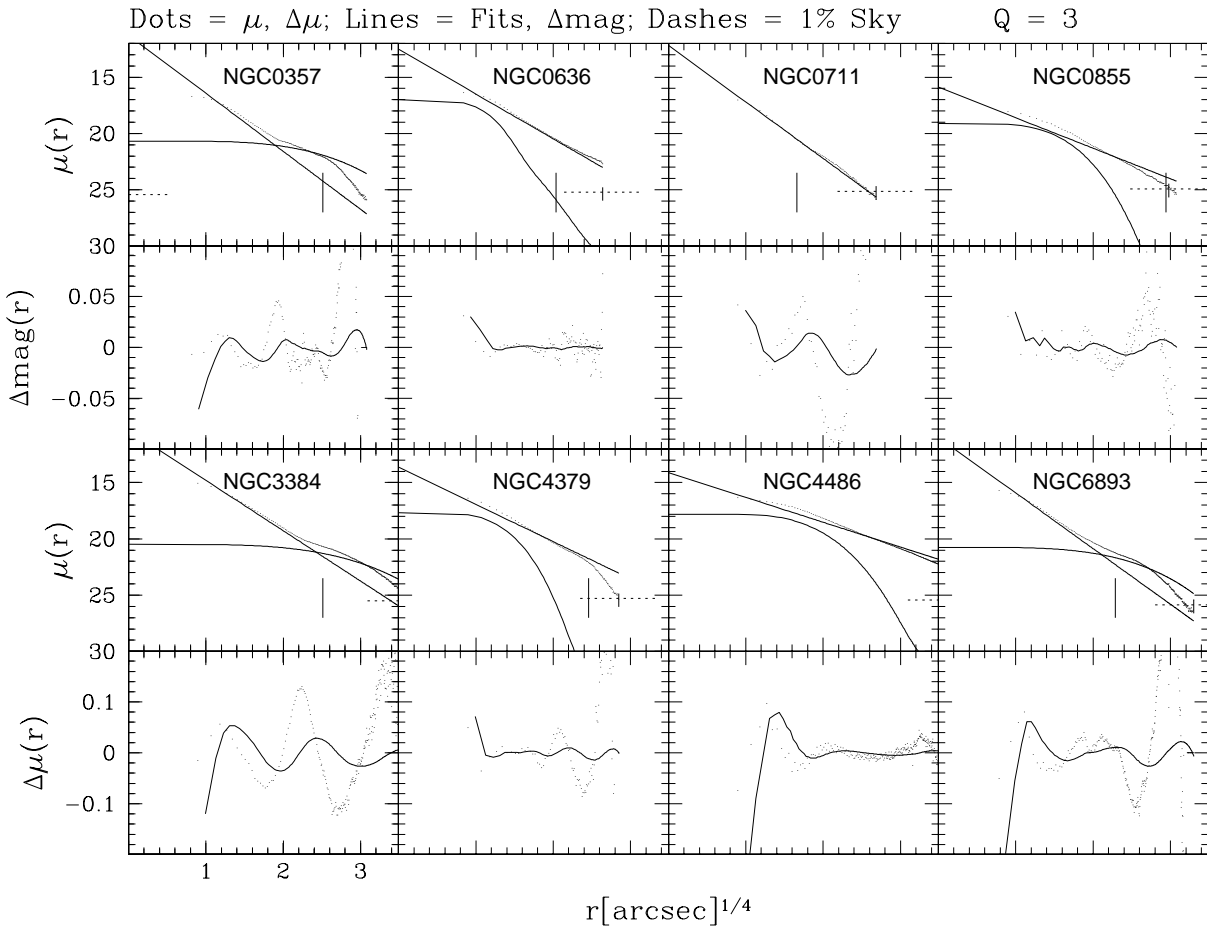


Fig. 5.— Examples of the light profile fitting of poor quality ($Q = 3$). The two panels for each galaxy show the observed light profile, the best fit and differences in surface brightness and magnitudes as in Figure 3.

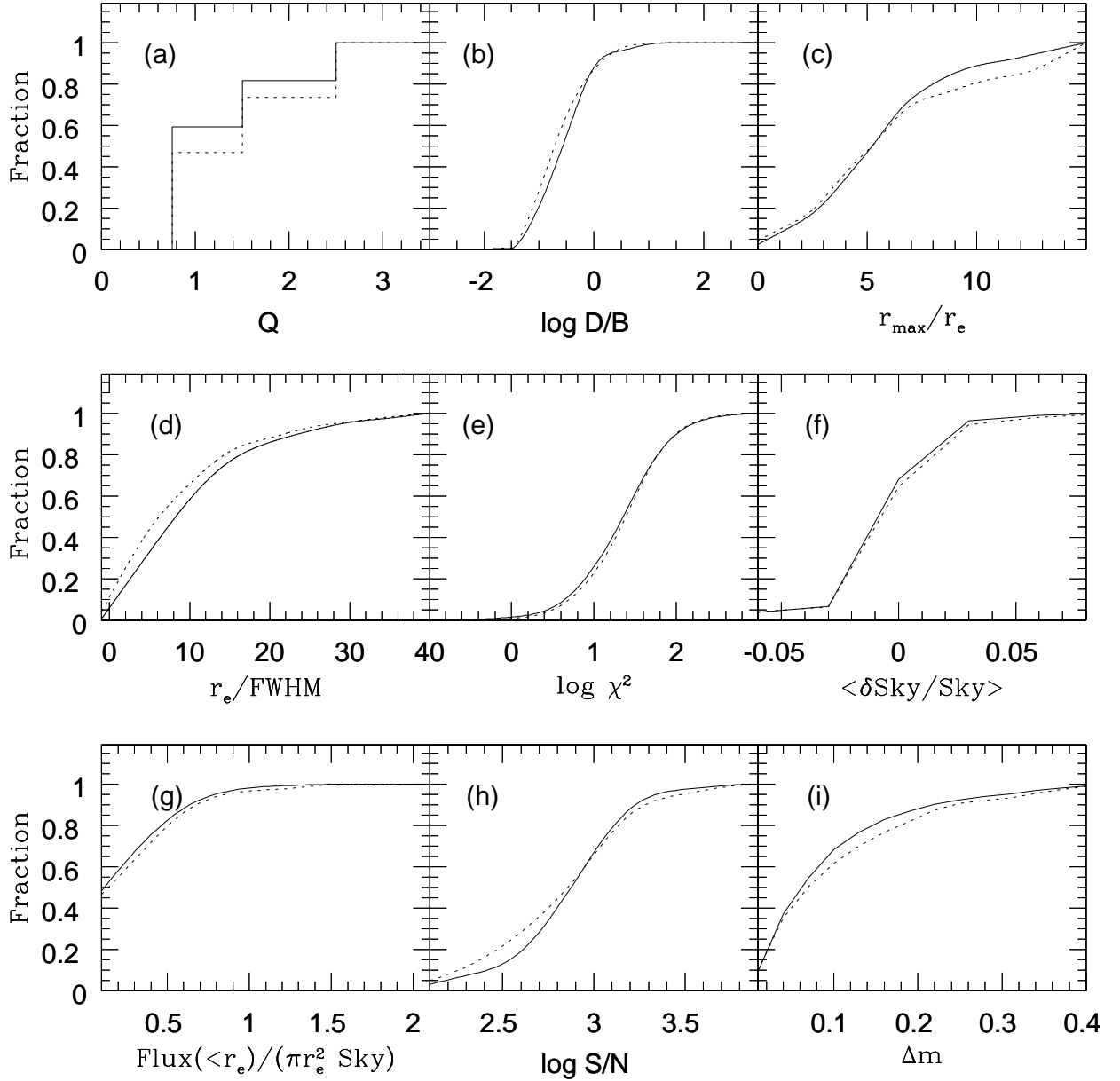


Fig. 6.— Cumulative distribution of the parameters which are obtained from the surface brightness

profile fits. The full line represents the ENEARm sample and the dashed line ENEARc. The panels

show the following parameters: in panel (a) the fit quality Q ; (b) the logarithm of the disk-to-bulge

ratio ($\log D/B = -1$ for simple $r^{1/4}$ fits); (c) the maximum extent of the profile (r_{max}) compared

to r_e ; (d) the ratio between r_e and the fitted PSF FWHM; (e) the logarithm of the reduced χ^2 of

the fit; (f) the average sky correction, whenever applicable; (g) the ratio between the flux of the

galaxy and the sky within r_e ; (h) the logarithm of the total signal-to-noise ratio of the profiles; and

(i) the amount of extrapolation used to compute the total magnitudes.

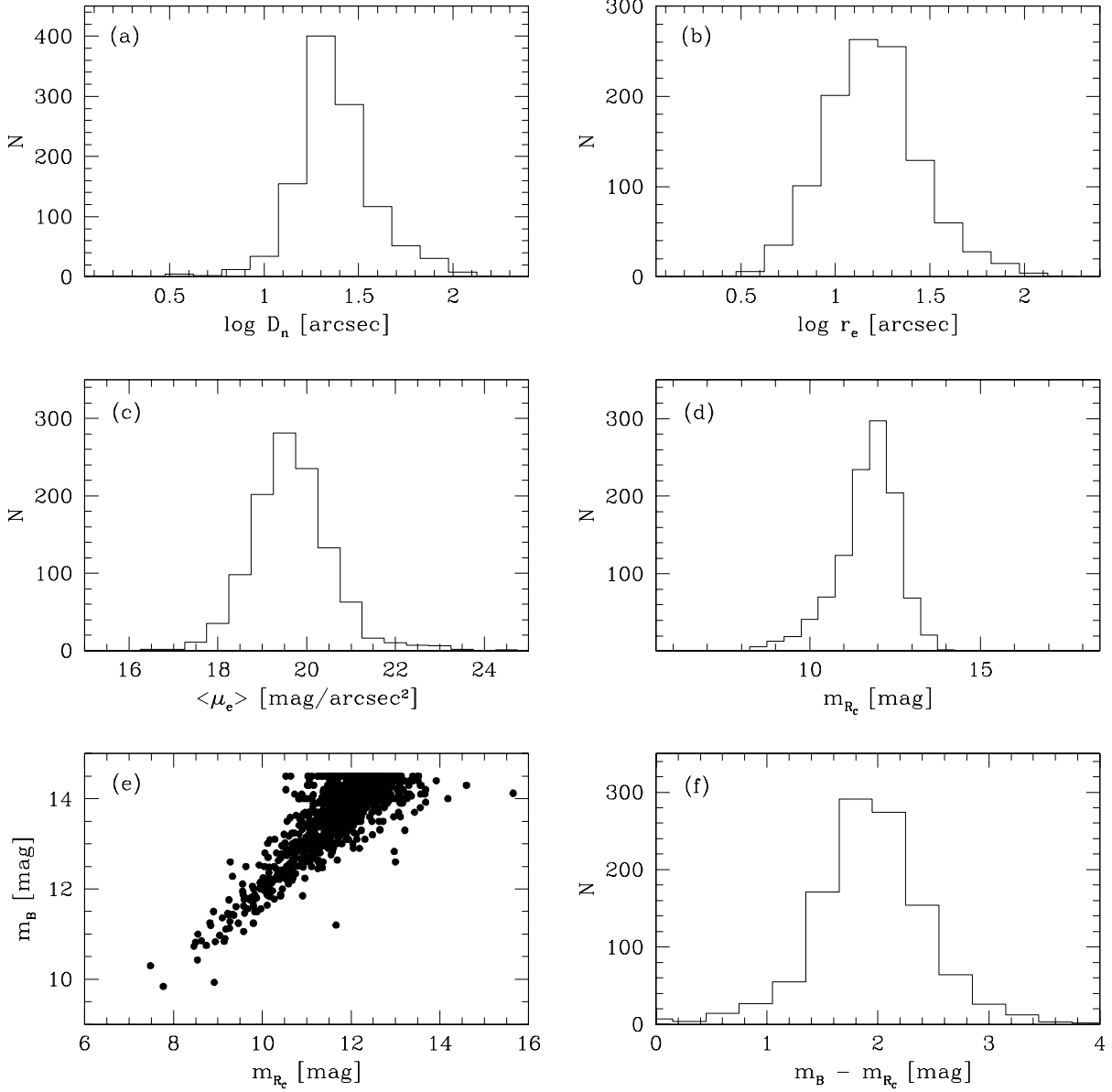


Fig. 7.— Distribution of the photometric parameters derived for the ENEARm sample. The D_n parameter is shown in arc seconds so that it may be directly compared to r_e . The panel (e) shows the B-band versus the R_C -band total magnitude and the panel (f) the distribution of the color B- R_C .

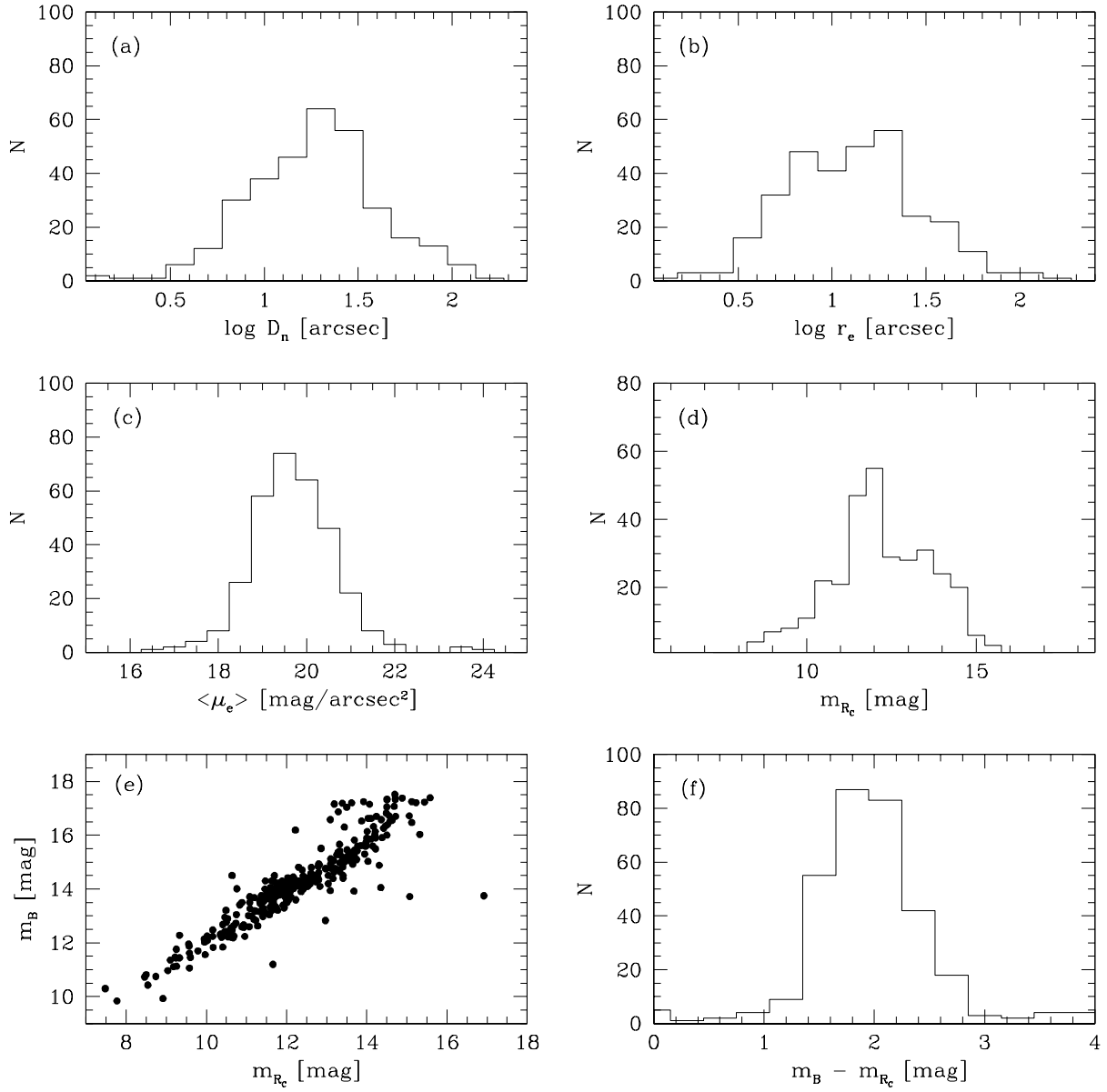


Fig. 8.— The same plots of Figure 7 for galaxies in clusters (ENEARc sample)

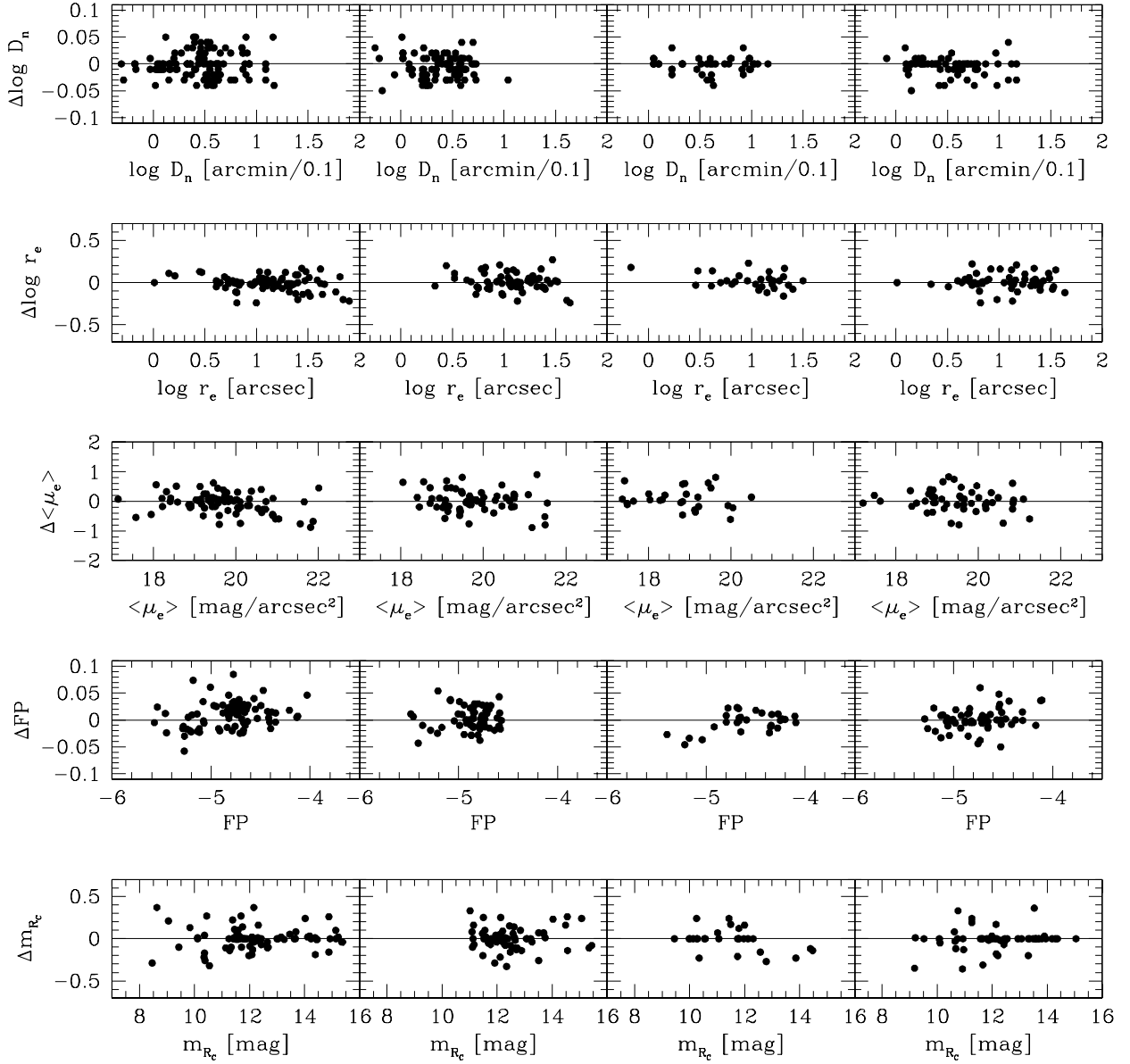


Fig. 9.— Internal comparisons of $\log D_n$, $\log r_e$, $\langle \mu_e \rangle$, FP, and m_{R_c} derived from data observed at ESO, MDM, FLWO and CTIO (panels from left to right, respectively).

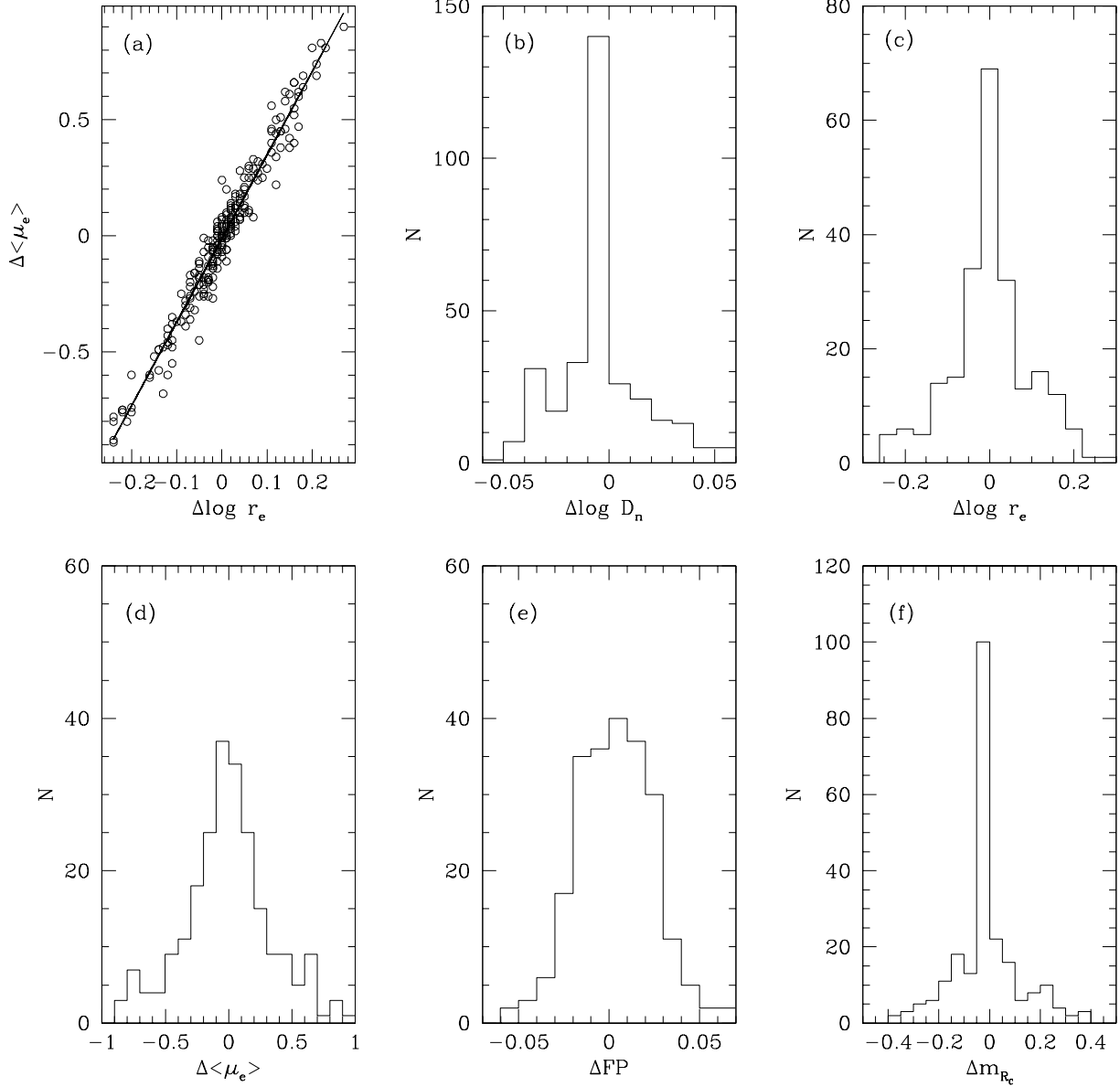


Fig. 10.— The distribution of the differences between parameters derived from our internal comparison: (Panel a) shows the correlation of the differences in $\log r_e$ and $\langle \mu_e \rangle$ and the solid line is the expected relation $\log r_e = 0.27 \langle \mu_e \rangle$. The histograms of the differences are shown in (Panel b) $\log D_n$, (Panel c) $\log r_e$, (Panel d) $\langle \mu_e \rangle$, (Panel e) FP and (Panel f) m_{R_c} .

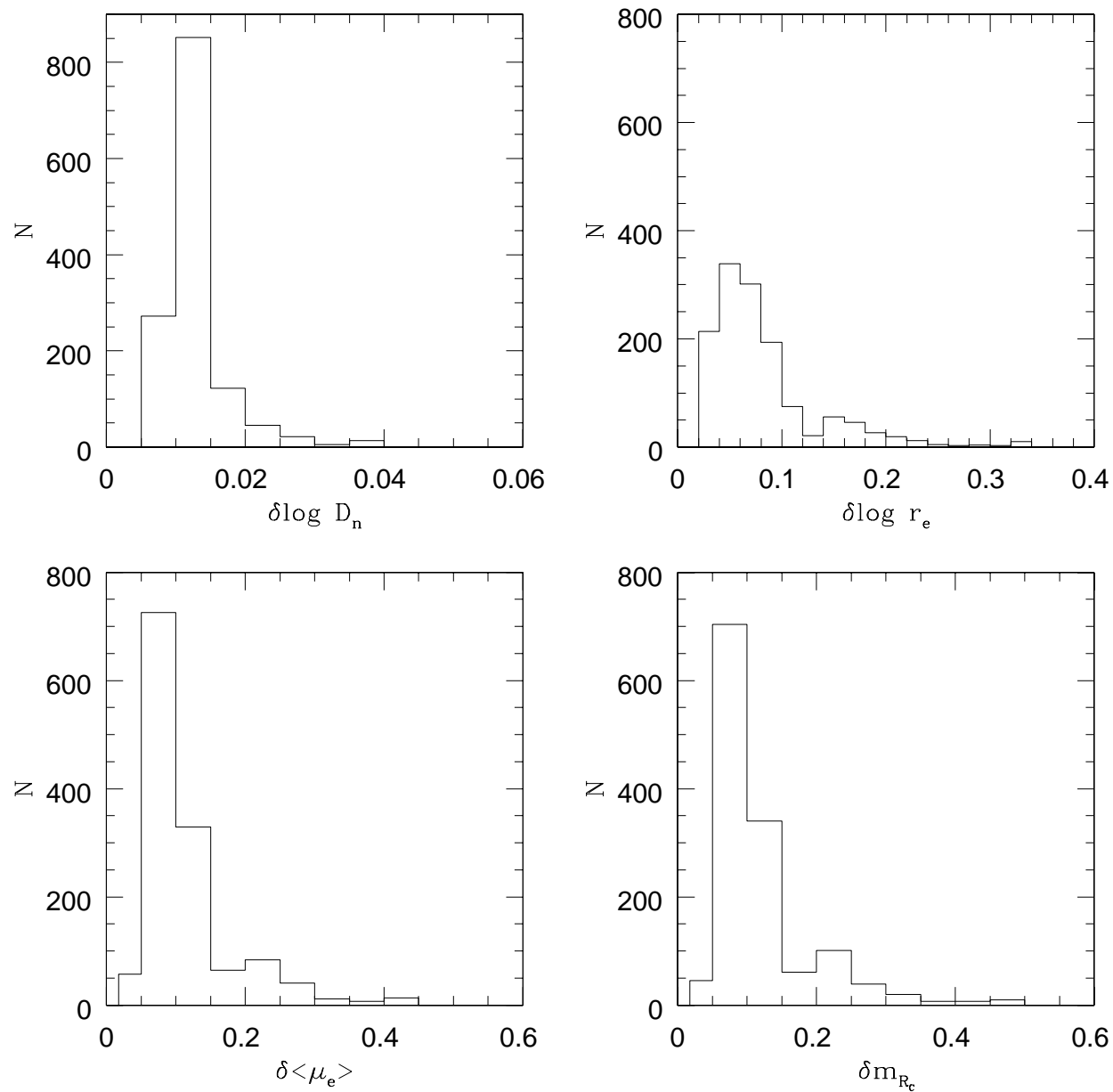


Fig. 11.— The distribution of the errors of the following parameters, obtained as explained in Section 3.2.3: (Panel a) $\log D_n$, (Panel b) $\log r_e$, (Panel c) $\langle \mu_e \rangle$, and (Panel d) m_{Rc} .

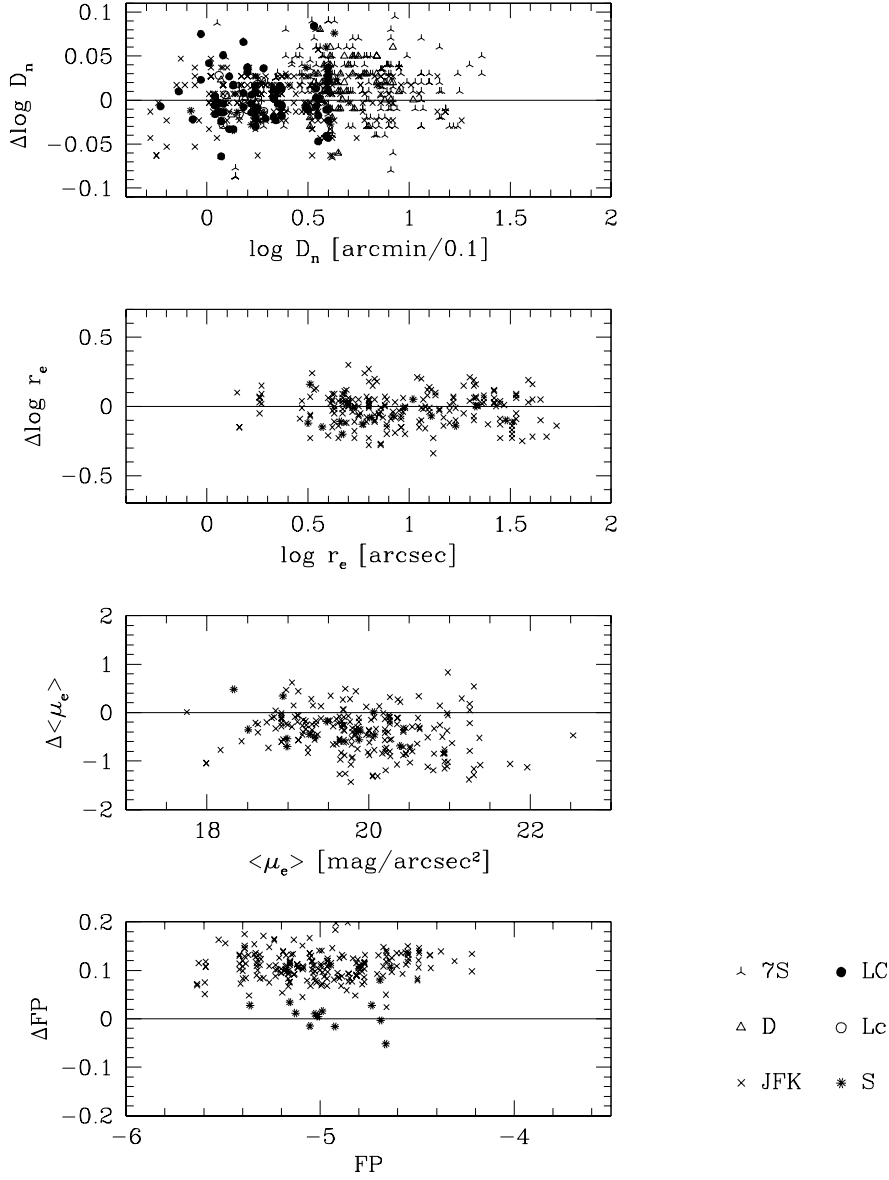


Fig. 12.— The overall external comparison of $\log D_n$, $\log r_e$, $\langle \mu_e \rangle$, and FP derived from our data. Δ means “ours-literature” measurements. The literature sources are: LC, Lucey & Carter (1988); 7S, Faber et al. (1989); D, Dressler (1987) and Dressler, Faber & Burstein (1991); JFK, Jørgensen, Franx, & Kjærgaard (1995); Lc, Lucey et al. (1997); and S, Smith et al. (1997).

Table 6. The Photometric ENEAR Catalog

name	α	δ	T	m_B	cz_{hel}	N_{obs}	m_{RC}	$\epsilon_{m_{RC}}$	$\log D_n$	ϵ_{D_n}	$\log r_e$	ϵ_{r_e}	$\langle \mu_e \rangle$	$\epsilon_{\langle \mu_e \rangle}$	D/B	FWHM	Notes	Lit
	(2000)	(2000)		mag	km s ⁻¹		mag		arcmin/0.1		arcsec		mag/arcsec ²			arcsec		
	(2)	(3)	(4)	(5)	(6)	(7)	(8)	(9)	(10)	(11)	(12)	(13)	(14)	(15)	(16)	(17)	(18)	(19)
C7805	00:01:27.1	+31:26:02	-2	14.30	4948	1	12.75	0.05	0.490	0.010	0.71	0.04	18.25	0.05	0.17	0.64	1	
C7810	00:02:19.3	+12:58:16	-2	14.30	5532	1	12.26	0.09	0.520	0.012	1.10	0.07	19.66	0.09	0.24	1.35	1	
C7832	00:06:28.4	-03:42:58	-3	13.50	6204	1	11.72	0.11	0.570	0.012	1.25	0.08	19.95	0.11	0.05	1.94	2	
C00061	00:07:23.8	+47:02:26	-2	14.30	5277	1	12.06	0.30	0.580	0.024	1.06	0.21	19.28	0.28	0.00	1.77	...	
C0043	00:13:00.8	+30:54:55	-2	13.90	4785	1	11.72	0.25	0.520	0.020	1.37	0.17	20.50	0.23	1.56	1.15	7	
C00130	00:13:56.9	+30:52:58	-7	14.20	4735	1	13.10	0.05	0.420	0.010	0.72	0.04	18.66	0.05	0.30	0.71	...	

Note. — The number in column (18) flags the following causes for features observed in the image and/or spectrum of a galaxy: (1) strong contamination by other galaxies along the line of sight, or interacting galaxies; (2) strong contamination by bright stars along the line of sight; (3) crowded background; (4) presence of spiral arms or shells; (5) presence of a bar; (6) presence of dust lanes; (7) high D/B ratio, edge-on galaxy; (8) presence of star formation; (9) peculiar shape, peculiar nucleus, presence of spikes; (10) faint galaxy; (11) D_n available in the literature but uncertain; (12) image problems: large masked region, saturation, large galaxy compared to the field-of-view, faint parts near the CCD limits; (13) presence of a bar or ring in the galaxy; (14) dwarf galaxy; (15) galaxy observed with poor seeing or elongated PSF; (16) peripheral cluster member.